Inorganic Chemistry

Article

pubs.acs.org/IC

Solvent-Dependent Formation of Os(0) Complexes by Electrochemical Reduction of [Os(CO)(2,2′-bipyridine)(L)Cl_2]; L = Cl^-, PrCN

Joanne Tory,[†] Lisa King,[†] Antonios Maroulis,[†] Matti Haukka,[‡] Maria José Calhorda,[§] and František Hartl*,[†]

[†]Department of Chemistry, University of Reading, Whiteknights, Reading, RG6 6AD, U.K.

[‡]Department of Chemistry, University of Jyväskylä, P.O.Box 35, FI-40014 Jyväskylä, Finland

[§]Departamento de Química e Bioquímica, CQB, Faculdade de Ciências da Universidade de Lisboa, Campo Grande, Ed. C8, 1749-016 Lisbon, Portugal

Supporting Information

ABSTRACT: Cyclic voltammetry and ultraviolet−visible/infrared (UV−vis/IR) spectroelectrochemistry were used to study the cathodic electrochemical behavior of the osmium complexes *mer*-[Os^{III}(CO) (bpy)Cl_3] (bpy = 2,2′-bipyridine) and *trans*(Cl)-[Os^{II}(CO) (PrCN)(bpy)Cl_2] at variable temperature in different solvents (tetrahydrofuran (THF), butyronitrile (PrCN), acetonitrile (MeCN)) and electrolytes (Bu_4NPF_6, Bu_4NCl). The precursors can be reduced to *mer*-[Os^{II}(CO) ($bpy^{\bullet-}$)Cl_3]$^{2-}$ and *trans*(Cl)-[Os^{II}(CO)(PrCN) ($bpy^{\bullet-}$)Cl_2]$^-$, respectively, which react rapidly at room temperature, losing the chloride ligands and forming Os(0) species. *mer*-[Os^{III}(CO) (bpy)Cl_3] is reduced in THF to give ultimately an Os−Os-bonded polymer, probably [Os^0(CO) (THF)-(bpy)]$_n$, whereas in PrCN the well-soluble, probably mononuclear [Os^0(CO) (PrCN)(bpy)], species is formed. The same products were observed for the 2 electron reduction of *trans*(Cl)-[Os^{II}(CO)(PrCN) (bpy)Cl_2] in both solvents. In MeCN, similar to THF, the [Os^0(CO) (MeCN)(bpy)]$_n$ polymer is produced. It is noteworthy that the bpy ligand in mononuclear [Os^0(CO) (PrCN)(bpy)] is reduced to the corresponding radical anion at a significantly less negative potential than it is in polymeric [Os^0(CO) (THF)(bpy)]$_n$: $\Delta E_{1/2}$ = 0.67 V. Major differences also exist in the IR spectra of the Os(0) species: the polymer shows a broad ν(CO) band at much smaller wavenumbers compared to the soluble Os(0) monomer that exhibits a characteristic ν(*Pr*-CN) band below 2200 cm^{-1} in addition to the intense and narrow ν(CO) absorption band. For the first time, in this work the M^0-bpy (M = Ru, Os) mono- and dicarbonyl species soluble in PrCN have been formulated as a mononuclear complex. Density functional theory (DFT) and time-dependent-DFT calculations confirm the Os(0) oxidation state and suggest that [Os^0(CO) (PrCN)(bpy)] is a square planar moiety. The reversible bpy-based reduction of [Os^0(CO) (PrCN)(bpy)] triggers catalytic reduction of CO_2 to CO and $HCOO^-$.

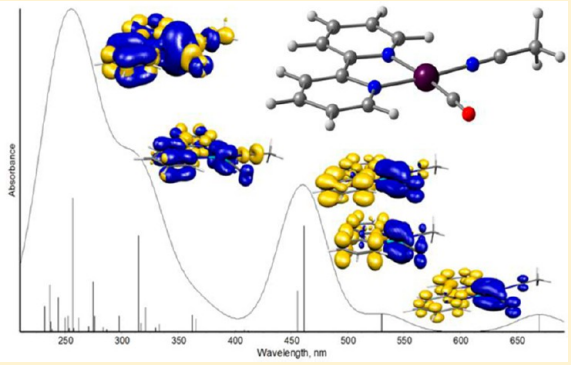

INTRODUCTION

Complexes of the type [M(CO) (bpy)(L)Cl_2] (M = Ru, Os; bpy = 2,2′-bipyridine; L = CO, RCN, Cl) are of longstanding interest as precursors of electro- and photocatalysts for the reduction of CO_2.[1] For example, electropolymerization of *mer*-[Ru^{II}(CO) (bpy)Cl_3]$^-$ in MeCN containing 5% water produced a Ru(0) species that was originally assigned as [{Ru^0(CO) (bpy)Cl}$^-$]$_n$. Exhaustive electrolysis with CO_2 in solution led to quantitative production of CO, and when the catalyst was prepared as a thin film on a carbon-felt working electrode, CO was produced with a 60% faradaic yield.[2]

Electrochemical reduction of two monocarbonyl ruthenium complexes, *mer*-[Ru^{III}(CO) (bpy)Cl_3] and *cis*(Cl)-[Ru^{II}(CO)-(MeCN) (bpy)Cl_2], was recently monitored with infrared (IR) and ultraviolet−visible (UV−vis) spectroelectrochemistry. It has been proposed that reduction of *mer*-[Ru(CO) (bpy)Cl_3] in tetrahydrofuran (THF) produces [{Ru^0(CO) (bpy)Cl}$^-$]$_n$ (eqs 1−4), whereas [Ru^0(CO) (PrCN)(bpy)]$_n$ forms in butyronitrile (PrCN, C_3H_7CN) as the stronger coordinating solvent.

$$mer\text{-}[Ru^{III}(CO)(bpy)Cl_3] + e^- \leftrightarrow mer\text{-}[Ru^{II}(CO)(bpy)Cl_3]^- \quad (1)$$

$$mer\text{-}[Ru^{II}(CO)(bpy)Cl_3]^- + e^- \rightarrow [Ru^{II}(CO)(bpy^{\bullet-})Cl_3]^{2-} \quad (2)$$

Received: August 27, 2013
Published: January 13, 2014

   dx.doi.org/10.1021/ic402146t | *Inorg. Chem.* 2014, 53, 1382−1396

$$n[Ru^{II}(CO)(bpy^{\bullet-})Cl_3]^{2-} + 2ne^- \rightarrow [\{Ru^0(CO)(bpy^{\bullet-})Cl\}^{2-}]_n + 2nCl^- \quad (3)$$

$$[\{Ru^0(CO)(bpy^{\bullet-})Cl\}^{2-}]_n \leftrightarrow [\{Ru^0(CO)(bpy)Cl\}^{-}]_n + ne^- \quad (4)$$

The presence of a chloride ligand in a reduced Ru(0) monocarbonyl complex is, however, highly unusual. The Ru−Cl bond is likely to dissociate at the electron-rich Ru(0) center, especially if the complex bears an overall negative charge. For both *mer*-$[Ru^{III}(CO)(bpy)Cl_3]$ and *cis*(Cl)-$[Ru^{II}(CO)(MeCN)(bpy)Cl_2]$, the expected "polymer" $[Ru^0(CO)(PrCN)(bpy)]_n$ formed in PrCN was found to be significantly more soluble than that in THF, even in the bpy-reduced anionic form.[3]

A similar difference in solubility was observed for the Os(0) polymer product generated by electrochemical reduction of *trans*(Cl)-$[Os^{II}(CO)_2(bpy)Cl_2]$, which is soluble in PrCN but not in THF or acetonitrile (MeCN) where it deposits on the cathode as a dark insoluble film.[4] IR spectroelectrochemistry has provided some insight into this difference. In THF, the strong ν(CO) bands of the parent complex at 2032 and 1962 cm^{-1} are replaced upon the reduction by broad, weak bands at 1958, 1901, and 1870 cm^{-1} attributed to the insoluble polymer $[Os^0(CO)_2(bpy)\}]_n$. The latter chain is ultimately reduced to $[\{Os^0(CO)_2(bpy^{\bullet-})\}^-]_n$, absorbing at 1930 and 1859 cm^{-1}. Reduction in PrCN at 248 K proceeds via the reactive anion $[Os^{II}(CO)_2(bpy^{\bullet-})Cl_2]^-$ (ν(CO) at 2004 and 1928 cm^{-1}) converting to a soluble species with two fairly narrow and intense ν(CO) bands at 1940 cm^{-1} and 1855 cm^{-1},[4] and a previously unreported band at 2176 cm^{-1}, typical for a ν(CN) stretch of PrCN coordinated to a low-valent metal center.[5] The 3 electron (e^-)-reduced species has previously been attributed[4] to $[\{Os^0(CO)_2(bpy^{\bullet-})\}^-]_n$ in both solvents. However, the presence of the ν(CN) stretch at 2176 cm^{-1} and the absence of coordination sites available to bind the PrCN ligands in Os−Os-bonded $[\{Os^0(CO)_2(bpy)\}]_n$ suggest that it is actually a mononuclear species, stabilized by PrCN coordination.

The $2e^-$ electropolymerization of the analogous ruthenium dicarbonyl complex *trans*(Cl)-$[Ru^{II}(CO)_2(bpy)Cl_2]$ in weakly coordinating solvents such as THF is well understood. Intermediate dimeric, tetrameric, and oligomeric complexes are formed at similar reduction potentials as the parent complex, and films of the dark blue $[Ru(CO)_2(bpy)]_n$ polymer ultimately deposit on the conductive surface.[6] The structure of $[Ru(CO)_2(bpy)]_n$ has been the subject of X-ray powder diffraction,[7] solid-state NMR,[8] and DFT studies.[9] It has been estimated that $[Ru(CO)_2(bpy)]_n$ has a chain length of 20 monomer units and Ru−Ru bond distances of 2.95 Å. The Ru−Ru bonds are slightly longer than those found in the related linear polymer $[Ru(CO)_4]_n$.[10]

$[Ru(CO)_2(bpy)]_n$ films are of interest as a result of their high, electrochemically controlled conductivity[11] and their activity as catalysts for the reduction of CO_2.[1,2,12] Related metal complexes of the type $[Ru(CO)_2(NN)Cl_2]$ (NN = α-diimine) have recently been polymerized onto a range of semiconductors, including indium phosphide, gallium phosphide, and Cu_2ZnSnS_4, to produce hybrid photocatalysts capable of reducing CO_2 to formate in an aqueous environment. In a two-electrode system with a platinum-loaded anatase photocatalyst for water oxidation, CO_2 was photocatalytically reduced to formate under light irradiation with no external electrical bias and with a formate turn over number (TON) > 17 after 24 h.[13]

The osmium dicarbonyl complex *trans*(Cl)-$[Os^{II}(CO)_2(bpy)Cl_2]$ has also been shown to photocatalyze the reduction of CO_2 to CO.[1b]

Recent experiments[14] have shown that the reduction of *trans*(Cl)-$[Ru^{II}(CO)_2(bpy)Cl_2]$ to $[Ru(CO)_2(bpy)]_n$ in PrCN also produces a soluble Ru(0) species with a ν(CN) band at 2184 cm^{-1}, pointing to PrCN coordination at the Ru(0) center, similar to the reduction path of *trans*(Cl)-$[Os^{II}(CO)_2(bpy)Cl_2]$ in this solvent. It is important to understand and control the solubility in different solvents, as the preformed catalyst can be readily transported and deposited deliberately elsewhere.

The purpose of this cyclic voltammetric and spectroelectrochemical study is to investigate the electrochemical reductions of two osmium monocarbonyl complexes, *trans*(Cl)-$[Os^{II}(CO)(PrCN)(bpy)Cl_2]$ and the new *mer*-$[Os^{III}(CO)(bpy)Cl_3]$ complex (Chart 1), under different experimental conditions,

Chart 1. Structures of *mer*-$[Os^{III}(CO)(bpy)Cl_3]$ and *trans*(Cl)-$[Os^{II}(CO)(PrCN)(bpy)Cl_2]$ (bpy =2,2′-bipyridine, PrCN = C_3H_7CN)

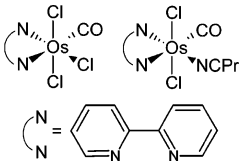

that is, varying the solvent, temperature, and supporting electrolyte. Comparison of the cathodic behavior of these complexes with that of the monocarbonyl ruthenium analogues and the $[M(CO)_2(bpy)Cl_2]$ complexes should give us greater insight into the true nature of the potential catalyst species.

The greater strength of the Os−Cl bond in comparison to the Ru−Cl bond leads to an increase in the stability of the intermediate species, making the osmium complexes useful for mechanistic studies,[15] particularly with regard to probing the existence of $[\{Os^0(CO)(bpy^{\bullet-})Cl\}^{2-}]_n$, the osmium analogue of a ruthenium polymer proposed for the reduction path of *mer*-$[Ru^{III}(CO)(bpy)Cl_3]$ in THF.[3]

DFT calculations were carried out to support the experimental data and reveal the nature of the Os(0) reduction products. Finally, the ability of these complexes to act as catalysts for the electrochemical reduction of CO_2 was also investigated with thin-layer IR spectroelectrochemistry.

EXPERIMENTAL SECTION

Materials and Preparations. All solvents were freshly distilled under a dry nitrogen atmosphere prior to use. THF was refluxed with Na wire and benzophenone; acetonitrile was refluxed with P_2O_5; butyronitrile was refluxed with CaH_2. The supporting electrolyte Bu_4NPF_6 (TBAPF$_6$, Aldrich) was recrystallized twice from absolute ethanol and dried in vacuum prior to use. All electrochemical and spectroelectrochemical measurements were carried out under an inert atmosphere of dry N_2 or Ar, using Schlenk techniques. Elemental analysis of *mer*-$[Os(bpy)Cl_3(CH_3OH)]$ was conducted with a Vario MICRO V1.7.0 CHNS Mode analyzer (Joensuu, Finland). Elemental analysis of *mer*-$[Os(CO)(bpy)Cl_3]$ was carried out by MEDAC Ltd. (UK).

mer-[Os(bpy)Cl$_3$(CH$_3$OH)]. The precursor of the monocarbonyl complex was synthesized by the same method as the corresponding ruthenium complex *mer*-$[Ru(bpy)Cl_3(CH_3OH)]$.[16] $OsCl_3 \cdot nH_2O$ (500 mg, ca. 1.43 mmol) was dissolved in methanol (50 mL). The solution was heated under reflux in a H_2 flow for 6 h until the black solution turned brownish green. 2,2′-Bipyridine (150 mg, 0.96 mmol) was added

dx.doi.org/10.1021/ic402146t | Inorg. Chem. 2014, 53, 1382−1396

to the solution and the mixture was refluxed under air for 18 h. The dark brown precipitate of *mer*-[Os(bpy)Cl_3(CH_3OH)] was filtered, dried under vacuum, and recrystallized from CH_3OH. The yield was 220 mg (0.57 mmol, ca. 40%). Single crystals of *mer*-[Os(bpy)Cl_3(CH_3OH)] suited for X-ray analysis (Figure S1, Supporting Information) were grown from CH_3OH. $C_{12}H_{16}Cl_3N_2O_2Os$ (516.82): Anal. Calcd C, 27.89; H, 3.12; N, 5.42; found C, 27.73; H, 3.04; N, 5.23%.

mer-[Os(CO)(bpy)Cl₃]. *mer*-[Os (bpy)Cl_3 (CH_3OH)]·CH_3OH (200 mg, 0.39 mmol) was dissolved in CH_2Cl_2 and introduced into a Berghof autoclave (100 mL) equipped with a Teflon liner. The autoclave was pressurized to 50 bar of CO and heated for 18 h at 60 °C. The carbonyl product was filtered and dried under vacuum. The yield of *mer*-[Os (CO)(bpy) Cl_3] was 130 mg (0.27 mmol, ca. 69%). Single crystals of the product were obtained from CH_2Cl_2. IR ν(CO) in KBr: 1992 cm^{-1}, ν(CO) in CH_2Cl_2: 2017 cm^{-1}, ν(CO) in PrCN: 2010 cm^{-1}. UV−vis (λ_{max} in PrCN): 300, 390, and 440(sh) nm. $C_{11}H_8Cl_3N_2OOs$ (480.74): Anal. Calcd C, 27.48; H, 1.68; N, 5.83; found C, 27.59; H, 1.74; N, 5.69%.

trans(Cl)-[Os(CO)(bpy)(PrCN)Cl₂]. This complex was prepared in situ in the pure form by the photochemical method described in the literature for *trans*(Cl)-[Os (CO)(bpy) (MeCN)Cl_2].[17] IR ν(CO) in PrCN: 1932 cm^{-1}. UV−vis (λ_{max} in PrCN): 298, 395, and 550 nm.

X-ray Structure Determination. The crystals of *mer*-[Os (bpy)-Cl_3 (CH_3OH)]·CH_3OH and *mer*-[Os (CO)(bpy) Cl_3] were immersed in cryo-oil, mounted in a Nylon loop, and measured at T = 100 K. The X-ray diffraction data were collected on a Nonius KappaCCD diffractometer using Mo Kα radiation (λ = 0.710 73 Å). The *EvalCCD*[18] program package was used for cell refinements and data reductions. The structure was solved by direct methods using the *SHELXS-97*[19] program. A semiempirical absorption correction based on equivalent reflections (*SADABS*)[20] was applied to the data. Structural refinements were carried out using *SHELXL-97*.[19] In [Os(CO) (bpy)Cl_3] the carbonyl ligand and the equatorial chloride (Cl1) were disordered over alternative sites with an occupancy ratio of 0.70/0.30. Because of the disorder, C and O atoms in the CO group were restrained to have similar U_{ij} components. In *mer*-[Os (bpy)Cl_3 (CH_3OH)]·CH_3OH the OH hydrogen atom was located from the difference Fourier map but constrained to ride on their parent atom, with U_{iso} = 1.5 × U_{eq}(parent atom). Other hydrogen atoms were positioned geometrically and constrained to ride on their parent atoms, with C−H = 0.95−0.98 Å and U_{iso} = 1.2−1.5 × U_{eq} (parent atom). The crystallographic details for *mer*-[Os(CO) (bpy)Cl_3] are summarized in Table 1 and Figure 1, and those for *mer*-[Os (bpy)Cl_3 (CH_3OH)]·CH_3OH can be found in Tables S1 and S2 (Supporting Information).

Cyclic Voltammetry. Cyclic voltammograms were recorded with an EG&G PAR Model 283 potentiostat operated with an M770 v.4.23 software. Airtight single-compartment three-electrode cells were used with a 0.422 mm^2 platinum microdisc working electrode polished with 0.25 μm diamond paste, a platinum wire auxiliary electrode, and a Ag wire pseudoreference electrode. The ferrocene/ferrocenium (Fc/Fc^+) redox couple served as an internal reference for the determination of electrode potentials and comparison of ΔE_p values (indicating a slow electron transfer). Samples contained 10^{-3} M Os complex and 10^{-1} M supporting electrolyte.

Spectroelectrochemistry. IR spectroelectrochemical experiments were performed at room temperature (RT, 293 K) and low temperature (LT, 193 K), using a Bruker Vertex 70v FT-IR spectrometer equipped with a deuterated triglycine sulfate detector (RT) or connected to a Bio-Rad FTS 60 MCT detector (LT). UV−vis spectroelectrochemistry was performed using a Scinco S-3100 diode-array spectrophotometer.

Thin-layer UV−vis and IR spectroelectrochemistry were carried out with OTTLE cells[21] equipped with Pt minigrid working and auxiliary electrodes, a Ag microwire pseudoreference electrode and CaF_2 windows. The course of spectroelectrochemical experiments was monitored by thin-layer cyclic voltammetry conducted with a PA4 (Laboratory Devices, Polná, Czech Republic) potentiostat. Samples contained 10^{-3} M (UV−vis) and 3 × 10^{-3} M (IR) Os complex and 3 × 10^{-1} M supporting electrolyte (Bu_4NPF_6 or Bu_4NCl).

Computational Details. DFT calculations[22] were performed using the Amsterdam Density Functional (ADF) program package.[23]

Table 1. Crystal Data for *mer*-[Os(CO)(bpy)Cl_3]

empirical formula	$C_{11}H_8Cl_3N_2OOs$
molecular weight	480.74
T (K)	100(2)
λ (Å)	0.71073
crystal system	monoclinic
space group	Pn
a (Å)	8.1215(5)
b (Å)	6.7002(3)
c (Å)	12.3686(4)
β (deg)	104.791(3)
V (Å^3)	650.74(5)
Z	2
ρ_{calc} (mg/m^3)	2.453
μ(Mo Kα) (mm^{-1})	10.400
number of reflns.	12 864
unique reflns.	3691
GOF (F^2)	0.801
R_{int}	0.0215
$R1$ ($I \geq 2\sigma$)[a]	0.0127
w$R2$ ($I \geq 2\sigma$)[b]	0.0267

[a] $R1 = \sum||F_o| - |F_c||/\sum|F_o|$. [b] $wR2 = \{\sum[w(F_o^2 - F_c^2)^2]/\sum[w(F_o^2)^2]\}^{1/2}$.

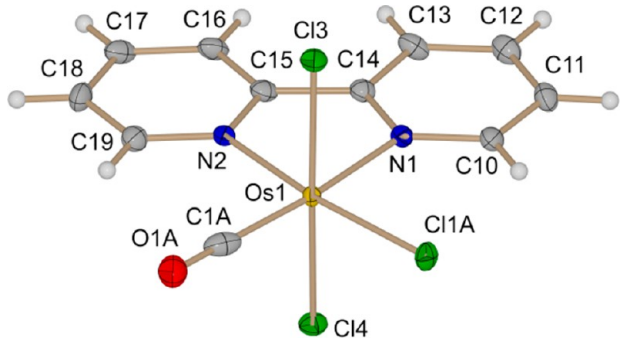

Figure 1. Crystal structure of *mer*-[Os(CO) (bpy)Cl_3] with thermal ellipsoids drawn at the 50% probability level and the atomic numbering scheme. Selected bond lengths (Å): Os(1)−N(1) 2.101(2); Os(1)−N(2) 2.079(2); Os(1)−Cl(1) 2.3300(15)(a), 2.322(4)(b); Os(1)−Cl(3) 2.322(4); Os(1)−Cl(4) 2.3345(6); Os(1)−C(1) 1.872(8)(a), 1.850(15)(b). Selected bond angles (deg): N(1)−Os(1)−N(2) 78.26(8); Cl(3)−Os(1)−Cl(4) 174.59(2); Cl(1)−Os(1)−O(1) 91.9(4)(a), 89.8(5)(b), where (a) = the 1A component of the disordered CO or Cl^- ligands and (b) = the 1B component of the disordered CO or Cl^- ligands.

Gradient-corrected geometry optimizations[24] (gas-phase and solvent) were performed without symmetry constraints, using the local density approximation of the correlation energy (Vosko-Wilk-Nusair)[25] augmented by the exchange-correlation functional of Becke and Perdew (BP86).[26] Triple-ζ Slater-type orbitals (STO) were used to describe the valence shells of N, C, O, H, and Os, with a set of two polarization functions (p,f for Os; d,f for Cl, N, C, O; and p,d for H). The core orbitals were frozen for Os ([1−4]s, [2−4]p, [3−4]d), Cl ([1−2]s, 2p), N, C, and O (1s). Unrestricted calculations were performed for paramagnetic species. The relativistic effects were treated with the ZORA approximation.[27] TD-DFT calculations were performed to determine electronic transitions (lowest 40−50).[28] Frequency calculations were performed for selected complexes and showed that all the species were minima in the potential energy surface. The solvent effects were included in all the calculations involving *mer*-[$Os^{II}Cl_3$ (CO)bpy]$^-$ and its reduced and oxidized derivatives, using the Conductor-like Screening Model (COSMO)[29] implemented in ADF. The rigid sphere radius of the NCMe solvent molecules was taken to be 2.76 Å,[30] and the

dx.doi.org/10.1021/ic402146t | *Inorg. Chem.* 2014, 53, 1382−1396

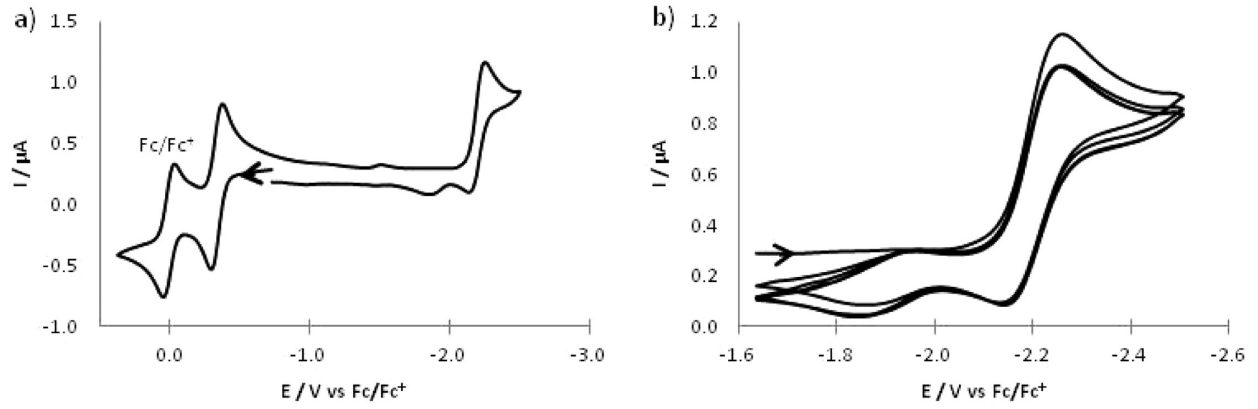

Figure 2. (a) Cyclic voltammogram of $[Os^{III}(CO)(bpy)Cl_3]$ in PrCN at T = 293 K. Scan rate = 100 mV s^{-1}. Because of the close position of the reversible Fc/Fc^+ and Os(III)/Os(II) redox couples, the scan started after potential equilibration with Os(II) at the working electrode surface. (b) Cathodic scan cycling of reduced $[Os^{II}(CO)(bpy)Cl_3]^-$ in PrCN. The less negative redox couple belongs to $[Os^0(CO)(PrCN)(bpy)]$ and its bpy-reduced form.

Table 2. Electrochemical Potentials (vs Fc/Fc^+) and Reduction Products of $[M(CO)(bpy)(L)Cl_2]$ (M = Ru[a], Os; L = Cl^-, PrCN)

		$E_{1/2}$ (Os^{II}/Os^{III})/V		$E_{1/2}$ (bpy/$bpy^{\bullet-}$)/V	
complex	solvent	293 K	213 K	293 K	213 K
$[Os(CO)(bpy)Cl_3]$	PrCN	−0.32	−0.24	−2.13	−2.13
	THF	−0.46	−0.44	−2.22	−2.24
trans(Cl)-$[Os(CO)(PrCN)(bpy)Cl_2]$	PrCN	+0.32	+0.42	−1.87	−1.87
$[Os(CO)(PrCN)(bpy)]$	PrCN			−1.88	
$[Os(CO)(THF)(bpy)]_n$	THF			−2.55	
mer-$[Ru(CO)(bpy)Cl_3]$	PrCN	+0.07		−2.08[b]	
	THF	−0.10		−2.29[b]	
cis(Cl)-$[Ru(CO)(PrCN)(bpy)Cl_2]$	PrCN	+0.67		−1.87[b]	−1.93[c]
$[Ru(CO)(PrCN)(bpy)]_n$[d]	PrCN			−1.93	
$[\{Ru(CO)(bpy)Cl\}^-]_n$[e]	THF			−2.51	

[a]Reference 3; potentials converted using the Fc/Fc^+ reference. [b]$E_{p,c}$ values. [c]An excess of Cl^- (3×10^{-1} M Bu_4NCl). [d]In fact, mononuclear $[Ru^0(CO)(PrCN)(bpy)]$. [e]In fact, most likely $[Ru^0(CO)(THF)(bpy)]_n$.

dielectric constant was 37.5. The van der Waals radii of the atoms were used for the atomic radius of the solute (or the atomic radius in the case of Os): Os 134 pm, Cl 175 pm, N 155 pm, C 170 pm, O 152 pm, H 120 pm.[31]

Three-dimensional representations of the orbitals were obtained with Molekel,[32] and structures, vibrational, and electronic spectra were obtained with Chemcraft.[33] The plots of the electron density difference maps obtained from TD-DFT calculations were based on the GausSum package,[34] modified to read the output of ADF.

RESULTS AND DISCUSSION

Characterization. The crystal structure for the orange solid *mer*-$[Os^{III}(CO)(bpy)Cl_3]$ in Figure 1 shows that, like *mer*-$[Ru^{III}(CO)(bpy)Cl_3]$, the complex has a slightly distorted octahedral structure with a meridional arrangement.[35] The crystal data is very similar to those obtained for both the analogous ruthenium complex[36] $[Ru^{III}(CO)(bpy)Cl_3]$ and the closely related dicarbonyl complex[37] *trans*(Cl)-$[Os^{II}(CO)_2(bpy)Cl_2]$. The Os−N and Os−Cl bonds are slightly shorter for $[Os^{III}(CO)(bpy)Cl_3]$[35]) than for *trans*(Cl)-$[Os^{II}(CO)_2(bpy)Cl_2]$, reflecting the higher oxidation state of the osmium center; whereas, there is a very small difference in the bond lengths between the Ru^{III} and Os^{III} complexes.

Cyclic Voltammetry of $[Os^{III}(CO)(bpy)Cl_3]$ in PrCN. Cyclic voltammetry was carried out to describe the electrochemical behavior of $[Os^{III}(CO)(bpy)Cl_3]$ and to determine similarities to the reduction path of *mer*-$[Ru^{III}(CO)(bpy)Cl_3]$.[3]

The cyclic voltammogram of $[Os^{III}(CO)(bpy)Cl_3]$ in PrCN at RT (Figure 2) shows a fully reversible redox couple at $E_{1/2}$ = −0.32 V (all potentials are recorded vs Fc/Fc^+) corresponding to the reduction of $[Os^{III}(CO)(bpy)Cl_3]$ to $[Os^{II}(CO)(bpy)Cl_3]^-$ (eq 5). This step is 0.39 V more negative than it is for the equivalent Ru(II)/Ru(III) couple (Table 2). This behavior is typical for Ru/Os-based oxidations, as can also be seen for example for *trans*(Cl)-$[M(CO)_2(bpy)Cl_2]$ (M = Ru, Os), where $\Delta E_{1/2}$ = 0.22 V.[3]

At ambient temperature (around 293 K), $[Os^{II}(CO)(bpy)Cl_3]^-$ undergoes partially chemically reversible $1e^-$ reduction (i_a/i_c = 0.78, scan rate = 100 mV s^{-1}) at $E_{1/2}$ = −2.13 V. For the reverse scan a second anodic peak is observed. Scan cycling shows the presence of a corresponding cathodic peak (Figure 2b), giving a new reversible redox couple at $E_{1/2}$ = −1.88 V. The peak current intensity of this redox couple slightly increased when the potential was held beyond the peak at $E_{1/2}$ = −2.13 V for several seconds (see Supporting Information, Figure S2).

Literature results[3] suggest that the ruthenium complex $[Ru^{II}(CO)(bpy)Cl_3]^-$ is reduced irreversibly in PrCN at $E_{p,c}$ = −2.08 V to give $[\{Ru^0(CO)(PrCN)(bpy^{\bullet-})\}^-]_n$ that can be reversibly oxidized to $[Ru^0(CO)(PrCN)(bpy)]_n$ at $E_{1/2}$ = −1.93 V. The electrochemical and spectroelectrochemical results (shown below) indicate that $[Os^{II}(CO)(bpy)Cl_3]^-$ and $[Ru^{II}(CO)(bpy)Cl_3]^-$ exhibit very similar behavior upon electrochemical reduction, although the bpy-based redox couples

dx.doi.org/10.1021/ic402146t | Inorg. Chem. 2014, 53, 1382−1396

at M(0) and M(II) are more separated; that is, ΔE = 0.25 and 0.15 V for M = Os and Ru, respectively.

The partially reversible cathodic wave at $E_{1/2}$ = −2.13 V has been assigned to bpy-based reduction of $[Os^{II}(CO)(bpy)Cl_3]^-$ that ultimately produces a negatively charged species, formulated on the basis of UV−vis/IR spectral data and DFT calculations (see below) as mononuclear $[Os^0(CO)(PrCN)(bpy^{\bullet-})]^-$ (eqs 6 and 7). The latter compound oxidizes at $E_{1/2}$ = −1.88 V to $[Os^0(CO)(PrCN)(bpy)]$ (eq 8).

$$[Os^{III}(CO)(bpy)Cl_3] + e^- \leftrightarrow [Os^{II}(CO)(bpy)Cl_3]^- \quad (5)$$

$$[Os^{II}(CO)(bpy)Cl_3]^- + e^- \rightarrow [Os^{II}(CO)(bpy^{\bullet-})Cl_3]^{2-} \quad (6)$$

$$[Os^{II}(CO)(bpy^{\bullet-})Cl_3]^{2-} + 2e^- + PrCN \rightarrow [Os^0(CO)(PrCN)(bpy^{\bullet-})]^- + 3Cl^- \quad (7)$$

$$[Os^0(CO)(PrCN)(bpy^{\bullet-})]^- \leftrightarrow [Os^0(CO)(PrCN)(bpy)] + e^- \quad (8)$$

The greater chemical reversibility of the reduction of $[M^{II}(CO)(bpy)Cl_3]^-$ to $[M^{II}(CO)(bpy^{\bullet-})Cl_3]^{2-}$ (M = Ru, Os) for the osmium center reflects the stronger Os−Cl bond compared to the Ru−Cl bond and, therefore, reflects the increased stability of $[Os^{II}(CO)(bpy^{\bullet-})Cl_3]^{2-}$. The value ΔE_p = 0.12 V for the $Os^0bpy/Os^0bpy^{\bullet-}$ couple is larger than ΔE_p = 0.08 V for the Os(II)/Os(III) redox couple (and the internal ferrocene/ferrocenium standard), revealing that the electron transfer is slower for the bpy-based reduction (an electrochemically quasireversible process), most likely due to concomitant structural changes in $[Os^{II}(CO)(bpy^{\bullet-})Cl_3]^{2-}$ preceding the dissociation of the chloride ligands.

The shift in the electrode potential of the $bpy/bpy^{\bullet-}$ couple for the M(II) complexes (M = Ru, Os) ($\Delta E_{p,c}$ = 0.14 V) is significantly smaller compared to the M(II)/M(III) couple, and the difference for the M(0) species $[M^0(CO)(PrCN)(bpy)]/[M^0(CO)(PrCN)(bpy^{\bullet-})]^-$ is not significant. This behavior reflects the smaller involvement of the metal in the redox process, so that the potential is less affected by changing the metal center.

In the cyclic voltammogram of $[Os(CO)(bpy)Cl_3]$ recorded at 213 K (Figure 3), the Os(II)/Os(III) and $bpy/bpy^{\bullet-}$ redox

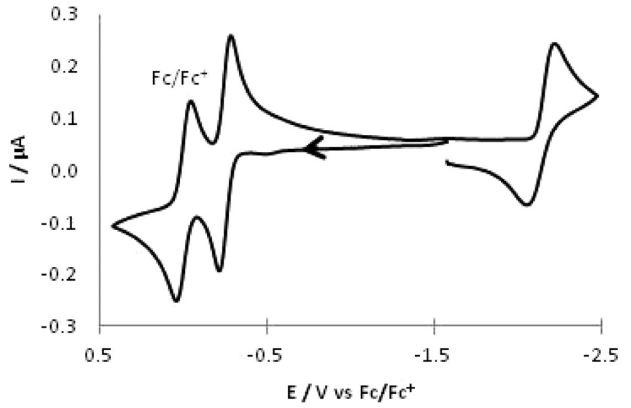

Figure 3. Cyclic voltammetry of $[Os^{III}(CO)(bpy)Cl_3]$ in PrCN at T = 213 K. Scan rate = 100 mV s^{-1}. Because of the close position of the reversible Fc/Fc^+ and Os(III)/Os(II) redox couples, the scan started after potential equilibration with Os(II) at the working electrode surface.

couples at $E_{1/2}$ = −0.24 V and $E_{1/2}$ = −2.13 V, respectively, are both chemically reversible as a result of the inherent stability of the primary $2e^-$-reduced product $[Os^{II}(CO)(bpy^{\bullet-})Cl_3]^{2-}$ at sufficiently low temperature. The electrochemically quasireversible nature of the latter process becomes more pronounced compared to the bpy reduction at 293 K (Figure 2).

Cyclic Voltammetry of $[Os^{III}(CO)(bpy)Cl_3]$ in THF. The complex $[Os^{III}(CO)(bpy)Cl_3]$ is reduced to stable $[Os^{II}(CO)(bpy)Cl_3]^-$ at $E_{1/2}$ = −0.43 V in THF at RT (eq 5). Subsequent partially chemically reversible reduction of $[Os^{II}(CO)(bpy)Cl_3]^-$ (i_a/i_c = 0.69 at ν = 100 mV s^{-1}) occurs at $E_{1/2}$ = −2.22 V (eqs 6 and 9, assignment discussed below). The new chemically reversible redox process at $E_{1/2}$ = −2.55 V (Figure 4) belongs to a

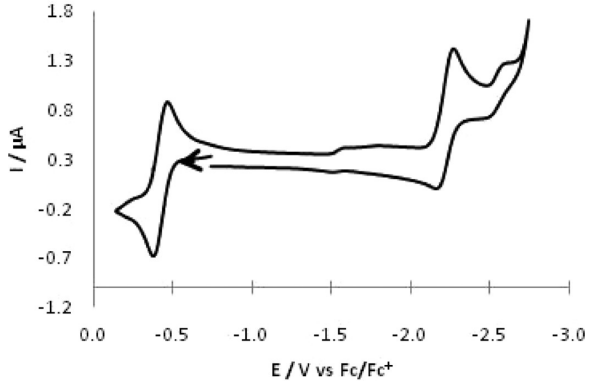

Figure 4. Cyclic voltammetry of $[Os^{III}(CO)(bpy)Cl_3]$ in THF. Scan rate =100 mV s^{-1}, T = 293 K. The scan started after potential equilibration with stable $[Os^{II}(CO)(bpy)Cl_3]^-$ at the working electrode surface.

secondary product, most likely an Os(0) polymer chain (eq 10), as concluded from spectroelectrochemical data below. This wave was not observed in the cyclic voltammograms recorded at temperatures below 253 K, where $[Os^{II}(CO)(bpy)Cl_3]^-$ becomes stable.

Comparison of the reduction of $[Os^{III}(CO)(bpy)Cl_3]$ in PrCN and THF reveals a significant difference of 0.67 V in the cathodic potentials of the secondary Os(0) species: in L = PrCN the $[Os^0(CO)(L)(bpy)]/[Os^0(CO)(L)(bpy^{\bullet-})]^-$ couple lies at a less negative potential than that of $[Os^{II}(CO)(bpy)Cl_3]^-/[Os^{II}(CO)(bpy^{\bullet-})Cl_3]^{2-}$; whereas, in THF the reduction of bpy ligand in the polymer is shifted to a more negative potential. It is very unlikely that chloride ligands remain bound to a highly reduced $Os^0(bpy^{\bullet-})$ species and, therefore, THF ligands have been proposed to complete the coordination sphere. The large negative shift in the reduction potential of the $Os^0(bpy)$ moiety cannot be explained by the simple substitution of PrCN for THF, supporting therefore the theory that the Os(0) product must have a different structure, namely, polymeric in THF and mononuclear in PrCN.

$$n[Os^{II}(CO)(bpy^{\bullet-})Cl_3]^{2-} + nTHF + ne^- \rightarrow [Os^0(CO)(THF)(bpy)]_n + 3nCl^- \quad (9)$$

$$[Os^0(CO)(THF)(bpy)]_n + ne^- \rightarrow [\{Os^0(CO)(THF)(bpy^{\bullet-})\}^-]_n \quad (10)$$

$[Os^{II}(CO)(bpy^{\bullet-})Cl_3]^{2-}$ can be reduced irreversibly at $E_{p,c}$ = −2.83 V (eq 11), resulting in enhanced formation of $[Os(CO)(THF)(bpy^{\bullet-})]_n$ (see Supporting Information, Figure S3) out of

dx.doi.org/10.1021/ic402146t | Inorg. Chem. 2014, 53, 1382−1396

very unstable $[Os^{II}(CO)(bpy^{2-})Cl_3]^{3-}$ losing rapidly the chloride ligands. The reduction of related $[Ru^{II}(CO)(bpy^{\bullet-})Cl_3]^{2-}$ was observed by cyclic voltammetry only at very low temperatures,[3] reflecting the weakness of the Ru−Cl bonds.

$$[Os^{II}(CO)(bpy^{\bullet-})Cl_3]^{2-} + e^- \rightarrow [Os^{II}(CO)(bpy^{2-})Cl_3]^{3-} \quad (11)$$

In summary, cyclic voltammetry shows that the electrolyte solution has a significant effect on the electrochemical behavior of $[Os^{III}(CO)(bpy)Cl_3]$. Spectroelectrochemistry was carried out in order to give greater insight into the different reduction products formed in THF and PrCN.

Spectroelectrochemistry of $[Os^{III}(CO)(bpy)Cl_3]$ in PrCN at 293 K. IR and UV−vis spectroelectrochemistry was employed to monitor the reduction of $[Os^{III}(CO)(bpy)Cl_3]$ in PrCN within an OTTLE cell at RT. The initial reduction $[Os^{III}(CO)(bpy)Cl_3]$ at −0.32 V shifted the ν(CO) band at 2010 cm^{-1} to 1899 cm^{-1} (Figure 5). This large shift agrees with the reversible Os−Cl-based reduction of $[Os^{III}(CO)(bpy)Cl_3]$ to $[Os^{II}(CO)(bpy)Cl_3]^-$ (eq 5) and largely increased Os-to-CO π-back-donation.

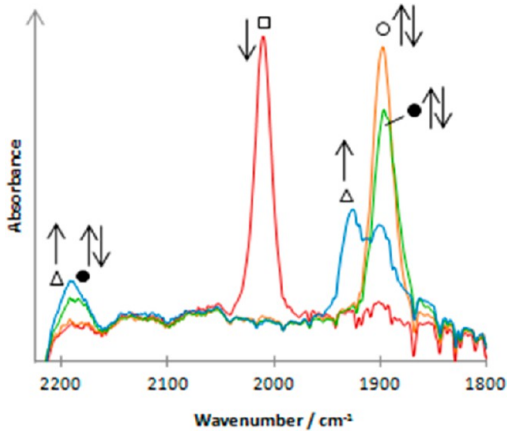

Figure 5. IR spectroelectrochemistry of $[Os^{III}(CO)(bpy)Cl_3]$ (□) in PrCN at 293 K within an OTTLE cell, showing its stepwise reduction to $[Os^{II}(CO)(bpy)Cl_3]^-$ (○) and $[Os^0(CO)(PrCN)(bpy^{\bullet-})]^-$ (●). Subsequent oxidation of the latter species leads to $[Os^0(CO)(PrCN)(bpy)]$ (△) and a partial recovery of $[Os^{II}(CO)(bpy)Cl_3]^-$.

Passing the second cathodic wave at −2.13 V (Figure 2) resulted in the shift of the carbonyl band to 1895 cm^{-1}. This change of merely 4 cm^{-1} from the ν(CO) wavenumber of $[Os^{II}(CO)(bpy)Cl_3]^-$ indicates that the product cannot be $[Os^{II}(CO)(bpy^{\bullet-})Cl_3]^{2-}$, which is expected to absorb at a much smaller ν(CO) wavenumber (viz. 1858 cm^{-1}, see below). This band is absent at low temperature where $[Os^{II}(CO)(bpy^{\bullet-})Cl_3]^{2-}$ becomes stable and in THF for the same irreversible process. The simultaneous appearance of a band at 2183 cm^{-1} was also observed, which is assigned to the C≡N stretch of butyronitrile (ν(*Pr*-CN)) coordinated at an Os(0) center. Its presence has been taken as evidence for the formation of the bpy-reduced mononuclear species $[Os^0(CO)(PrCN)(bpy^{\bullet-})]^-$ (eqs 6 and 7).

The UV−vis absorption bands of $[Os^{III}(CO)(bpy)Cl_3]$ at 300, 390, and 440(sh) nm were replaced upon the reduction of $[Os^{III}(CO)(bpy)Cl_3]$ to $[Os^{II}(CO)(bpy)Cl_3]^-$ by absorption bands at 299, 420, 465(sh), and 658 nm (Figure 6). Further reduction (Figure 7) produced a species with a UV−vis

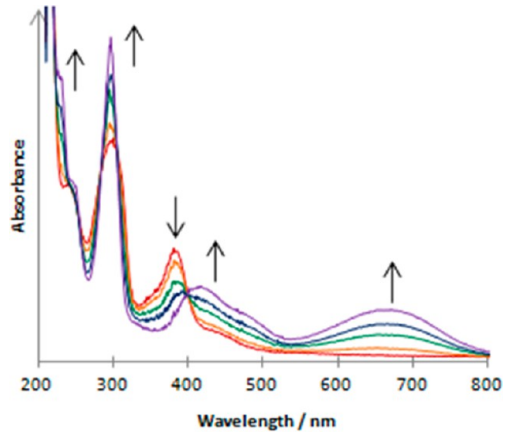

Figure 6. UV−vis spectroelectrochemistry showing the reduction of $[Os^{III}(CO)(bpy)Cl_3]$ to $[Os^{II}(CO)(bpy)Cl_3]^-$ in PrCN at 293 K within an OTTLE cell.

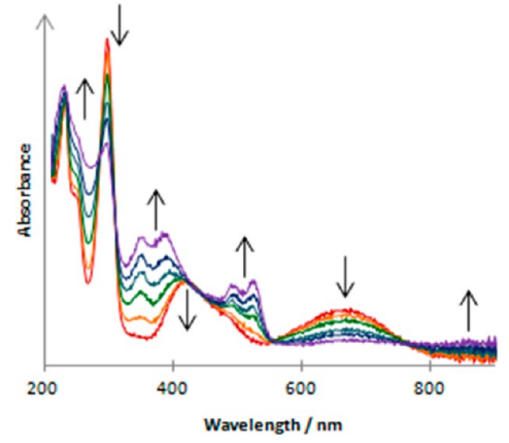

Figure 7. UV−vis spectroelectrochemistry showing the reduction of $[Os^{II}(CO)(bpy)Cl_3]^-$ to $[Os^0(CO)(PrCN)(bpy^{\bullet-})]^-$ in PrCN at 293 K within an OTTLE cell.

absorption spectrum showing typical[38] intraligand absorptions of $[bpy^{\bullet-}]$, namely, a bifurcated $\pi^*\pi^*$ band at 490 and 523 nm and weak $\pi^*\pi^*$ absorption in the NIR region below 800 nm. In addition, new bands arose also at 352 and 386 nm.

The singly reduced bpy ligand may correspond with the formation of either the dianion $[Os^{II}(CO)(bpy^{\bullet-})Cl_3]^{2-}$ or the Os(0) species $[Os^0(CO)(PrCN)(bpy^{\bullet-})]^-$. The presence of the ν(CN) stretch and the small change in the ν(CO) wavenumber compared to $[Os^{II}(CO)(bpy)Cl_3]^-$ in the concomitantly recorded IR spectrum suggest that the product is $[Os^0(CO)(PrCN)(bpy^{\bullet-})]^-$.

Reverse oxidation of $[Os^0(CO)(PrCN)(bpy^{\bullet-})]^-$ resulted in the partial recovery of $[Os^{II}(CO)(bpy)Cl_3]^-$ and the formation of a new species with ν(CO) and ν(CN) bands shifted to 1927 cm^{-1} and 2194 cm^{-1}, respectively. Given the reversible nature of the corresponding anodic process at −1.88 V (Figure 2), the new species (identified by the ν(CN) stretch) has been assigned to neutral $[Os^0(CO)(PrCN)(bpy)]$ (eq 8). The UV−vis absorption spectrum (Figure 8) showed absorption bands rising at 300, 420, and 650 nm. These spectral data support the partial recovery of $[Os^{II}(CO)(bpy)Cl_3]^-$ (Figure 5). The underlying electronic absorption of $[Os^0(CO)(PrCN)(bpy)]$ in the visible region (absorption maxima at 412 and 590 nm, vide infra) is poorly resolved.

dx.doi.org/10.1021/ic402146t | *Inorg. Chem.* 2014, 53, 1382−1396

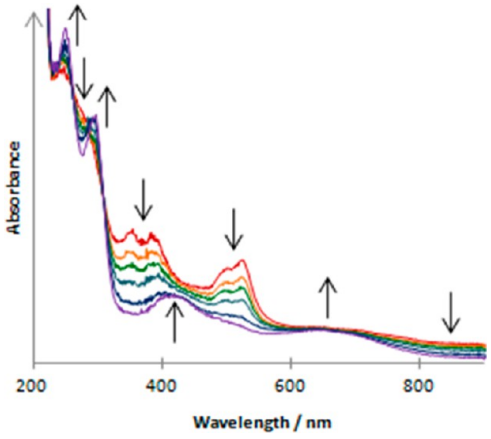

Figure 8. UV−vis spectroelectrochemistry showing the reoxidation of $[Os^0(CO)(PrCN)(bpy^{\bullet-})]^-$ to $[Os^0(CO)(PrCN)(bpy)]$ in PrCN at 293 K within an OTTLE cell. $[Os^{II}(CO)(bpy)Cl_3]^-$ is partly recovered.

Spectroelectrochemistry of $[Os^{III}(CO)(bpy)Cl_3]$ in PrCN at 213 K. Cyclic voltammetric scans suggest that the dianion $[Os^{II}(CO)(bpy^{\bullet-})Cl_3]^{2-}$ is stable at low temperatures (Figure 3). IR spectroelectrochemistry of $[Os^{III}(CO)(bpy)Cl_3]$ at 213 K was carried out within a low-temperature OTTLE cell to confirm this behavior.

Reduction of $[Os^{III}(CO)(bpy)Cl_3]$ to $[Os^{II}(CO)(bpy)Cl_3]^-$ in PrCN at 213 K results in the shift of the ν(CO) stretch from 2008 cm^{-1} to 1895 cm^{-1}. Further reduction at −2.17 V lowers the ν(CO) stretch to 1858 cm^{-1} and, unlike the reduction at 293 K, no ν(CN) band is observed (Figure 9). This important

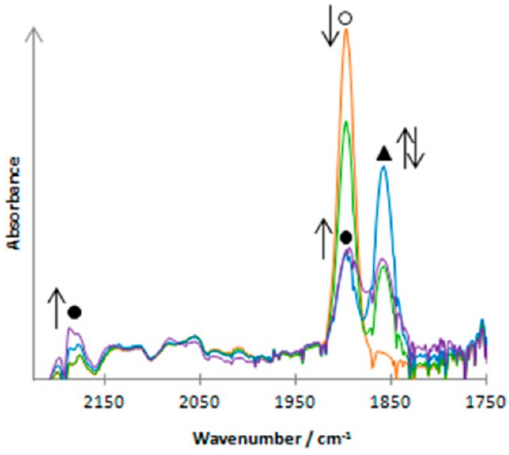

Figure 9. IR spectroelectrochemistry showing the reduction of $[Os^{II}(CO)(bpy)Cl_3]^-$ (○) to $[Os^{II}(CO)(bpy^{\bullet-})Cl_3]^{2-}$ (▲) and its subsequent conversion to $[Os^0(CO)(PrCN)(bpy^{\bullet-})]^-$ (●) in PrCN/$TBAPF_6$ at 213 K within an OTTLE cell.

difference reveals that the species formed is the primary radical complex $[Os^{II}(CO)(bpy^{\bullet-})Cl_3]^{2-}$ (eq 6). This product is still not completely stable at 213 K in PrCN/Bu_4NPF_6, converting slowly to the bpy-reduced mononuclear Os(0) species $[Os^0(CO)(PrCN)(bpy^{\bullet-})]^-$. This reaction was evidenced by the growth of a ν(CO) band at 1892 cm^{-1} accompanied by the ν(CN) stretch at 2181 cm^{-1} corresponding to the PrCN ligand coordinated at the Os(0) center (Figure 9).

Reduction of $[Os^{III}(CO)(bpy)Cl_3]$ at 213 K in PrCN/3 × 10^{-1} M Bu_4NCl containing a high excess of Cl^- shows a complete and reversible conversion of $[Os^{II}(CO)(bpy)Cl_3]^-$ to $[Os^{II}(CO)(bpy^{\bullet-})Cl_3]^{2-}$ (Figure 10). Slowly increasing the temperature of the solution results in a gradual transformation of

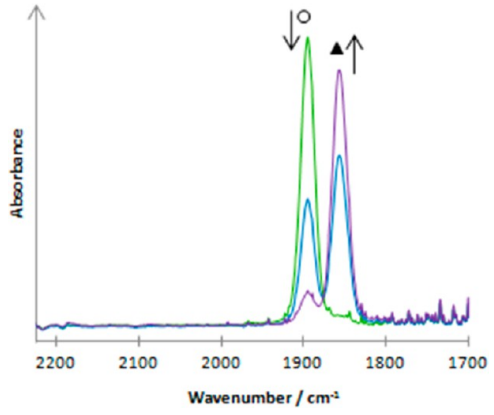

Figure 10. IR spectroelectrochemistry showing the complete cathodic conversion of $[Os^{II}(CO)(bpy)Cl_3]^-$ (○) to $[Os^{II}(CO)(bpy^{\bullet-})Cl_3]^{2-}$ (▲) in PrCN containing a high excess of Cl^- (3 × 10^{-1} M Bu_4NCl) at 213 K within an OTTLE cell.

$[Os^{II}(CO)(bpy^{\bullet-})Cl_3]^{2-}$ to $[Os^0(CO)(PrCN)(bpy^{\bullet-})]^-$ (not shown). UV−vis monitoring of the reversible reduction of $[Os^{II}(CO)(bpy)Cl_3]^-$ to $[Os^{II}(CO)(bpy^{\bullet-})Cl_3]^{2-}$ shows the appearance of an intense band at 368 nm and a characteristic bifurcated $\pi^*\pi^*(bpy^{\bullet-})$ band at 502 and 533 nm, confirming the presence of the reduced bpy ligand (Figure 11). Note that the

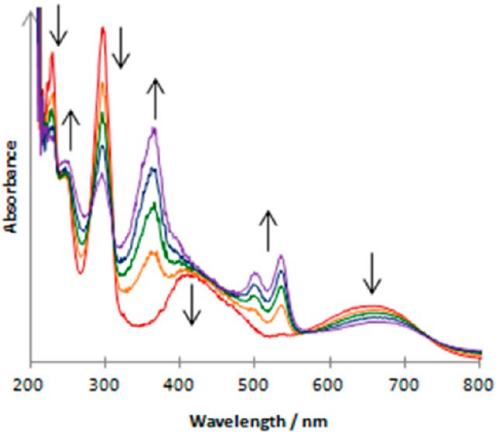

Figure 11. UV−vis spectroelectrochemistry showing the almost complete reduction of $[Os^{II}(CO)(bpy)Cl_3]^-$ to $[Os^{II}(CO)(bpy^{\bullet-})Cl_3]^{2-}$ in PrCN/3 × 10^{-1} M Bu_4NCl at 213 K within an OTTLE cell.

visible $\pi^*\pi^*(bpy^{\bullet-})$ absorption of related $[Os^{II}(CO)(PrCN)(bpy^{\bullet-})Cl_2]^-$ lies at a slightly lower energy and that of $[Os^0(CO)(PrCN)(bpy^{\bullet-})]^-$ lies at at a slightly higher energy (Table 3).

For comparison, the reduction of related $[Ru^{II}(CO)(bpy)Cl_3]^-$ at 198 K in PrCN/3 × 10^{-1} M Bu_4NCl gave a transient species in low concentration, which rapidly converted to stable $[Ru^0(CO)(PrCN)(bpy^{\bullet-})]^-$. The same experiment but without Cl^- in the electrolyte gave the transient species in a much lower concentration, and $[Ru^0(CO)(PrCN)(bpy^{\bullet-})]^-$ dominated from the very beginning. The short-lived product was originally assigned[3] as the polymer $[\{Ru^0(CO)(bpy)Cl\}^-]_n$, absorbing at the same IR ν(CO) wavenumber as the polymer obtained from the reduction of *mer*-$[Ru^{III}(CO)(bpy)Cl_3]$ in THF (assigned in

dx.doi.org/10.1021/ic402146t | Inorg. Chem. 2014, 53, 1382−1396

Table 3. IR and UV-Vis Experimental and DFT-Calculated Data for $[Os(CO)(bpy)(L)Cl_2]$ (L = Cl, PrCN) and Their Reduction Products

complex	solvent	ν(CO)/cm^{-1}	ν(CN)/cm^{-1}	λ_{max}/nm
$[Os^{III}(CO)(bpy)Cl_3]$	PrCN	2010		300, 390, 440(sh)
	PrCN	2008[a]		
	THF	2007		283, 388, 448(sh)
$[Os^{II}(CO)(bpy)Cl_3]^-$	PrCN	1899		299, 420, 465(sh), 658
	PrCN	1895[a]		
	THF	1903		296, 425, 473(sh), 685
				265(sh), 294, 441, 554, 710[b]
$[Os^{II}(CO)(bpy^{\bullet-})Cl_3]^{2-}$	PrCN	1858[a]		368, 394(sh), 502, 533[a]
$[Os^{II}(CO)(PrCN)(bpy)Cl_2]$	PrCN	1932		298, 395, 550
	PrCN	1931[a]		
	THF	1934		
$[Os^{II}(CO)(MeCN)(bpy)Cl_2]$[c]		1932		298, 362, 535
$[Os^{II}(CO)(MeCN)(bpy)Cl_2]$		1950[b]	2258[b]	283, 549, 846[b]
$[Os^{II}(CO)(PrCN)(bpy^{\bullet-})Cl_2]^-$	PrCN	1895[a]		360, 505, 540[a]
$[Os^{0}(CO)(PrCN)(bpy)]$	PrCN	1927	2194	289, 412, 590
$[Os^{0}(CO)(PrCN)(bpy^{\bullet-})]^-$	PrCN	1895	2183	352, 386, 490, 523, >700
	PrCN	1892[a]	2181[a]	
$[Os^{0}(CO)(THF)(bpy)]_n$	THF	1860(br)		280, 370, 515
$[Os^{-I}(CO)(MeCN)(bpy)]^-$		1827[b]	1938[b]	
$[Os^{0}(CO)(MeCN)(bpy)]$		1884[b]	2182[b]	256, 315, 462, 670[b]
$[Os^{I}(CO)(MeCN)(bpy)]^+$		1967[b]	2238[b]	

[a]At 213 K. [b]Theoretical values calculated with DFT. [c]Reference 17.

this work as $[Ru^0(CO)(THF)(bpy)]_n$). The longer lifetime of the polymer product in PrCN was ascribed to the higher stability of the Ru−Cl bond in the presence of excess Cl^-. However, a comparison with the spectroelectrochemical data obtained for the reduction path of $[Os^{III}(CO)(bpy)Cl_3]$ reveals that the reduced ruthenium transient species observed[3] in the cryostatted OTTLE cell was actually the primary reduction product $[Ru^{II}(CO)(bpy^{\bullet-})Cl_3]^{2-}$.

Spectroelectrochemistry of $[Os^{III}(CO)(bpy)Cl_3]$ in THF at 293 K. Reduction of $[Os^{III}(CO)(bpy)Cl_3]$ in THF was carried out to observe the differences between the mononuclear Os(0) species proposed to form in PrCN and the polymer produced in THF. For the corresponding ruthenium species $[Ru^{III}(CO)(bpy)Cl_3]$ it was proposed that the different polymer species $[Ru^0(CO)(PrCN)(bpy)]_n$ and $[\{Ru^0(CO)(bpy)Cl\}^-]_n$ were formed in PrCN and THF, respectively.[3] Cyclic voltammetry of $[Os^{III}(CO)(bpy)Cl_3]$ in THF (see above) suggests that the reduction of $[Os^{II}(CO)(bpy)Cl_3]^-$ at $E_{1/2}$ = −2.22 V results in the formation of a polymer with neutral bpy ligands that can be reduced further at $E_{1/2}$ = −2.55 V.

IR monitoring of the reduction of $[Os^{III}(CO)(bpy)Cl_3]$ in THF at 293 K shows a shift of the ν(CO) stretch at 2007 cm^{-1} first to 1903 cm^{-1} as $[Os^{III}(CO)(bpy)Cl_3]$ is reduced to $[Os^{II}(CO)(bpy)Cl_3]^-$. Subsequent reduction of $[Os^{II}(CO)(bpy)Cl_3]^-$ (Figure 12) led to the appearance of a broad low intensity ν(CO) band at 1860 cm^{-1}. Parallel UV−vis spectroelectrochemistry shows new poorly resolved absorption bands at 280, 370, and 515 nm forming upon the reduction of $[Os^{II}(CO)(bpy)Cl_3]^-$ (Figure 13). This UV−vis absorption spectrum is significantly different from that observed for $[Os^0(CO)(PrCN)(bpy^{\bullet-})]^-$ in PrCN (Figure 7), showing, as expected, no indication of the $bpy^{\bullet-}$ ligand (i.e., the absence of the characteristic $\pi^*\pi^*(bpy^{\bullet-})$ absorption in the visible−near-IR region).

The broad and fairly weak ν(CO) band at 1860 cm^{-1} observed for the reduction of $[Os^{II}(CO)(bpy)Cl_3]^-$ in THF at 293 K

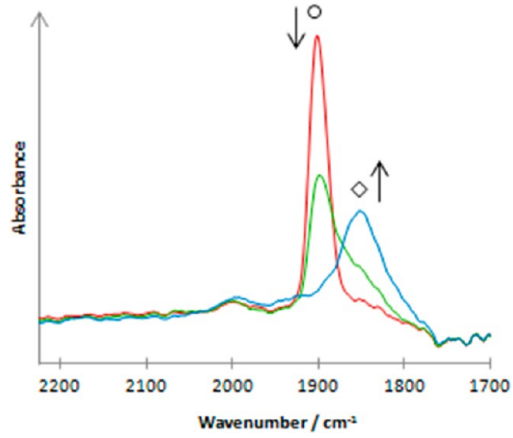

Figure 12. IR spectroelectrochemistry showing the reduction of $[Os^{II}(CO)(bpy)Cl_3]^-$ (○) to $[Os^0(CO)(THF)(bpy)]_n$ (◇) in THF at 293 K within an OTTLE cell.

(Figure 12) points to the formation of a polymeric species. The low intensity indicates its limited solubility compared to the well-soluble Os(0) species formed in PrCN; whereas, the width is likely to reflect a variable chain length in the polymer and different local conformations and environments existing along the polymer chain, as revealed by the X-ray structure in the case of the well-known related polymer $[Ru(CO)_2(bpy)]_n$.[7]

The instability of the Os−Cl bond at RT for the bpy-reduced osmium(II) complexes suggests that an Os(0) polymer species with a bound chloride ligand is highly unlikely. Instead, a THF solvent molecule is likely to bind at the Os(0) center, producing $[Os^0(CO)(THF)(bpy)]_n$ (eqs 6 and 9). Further reduction of $[Os^0(CO)(THF)(bpy)]_n$ at −2.55 V led to decomposition indicated by appearance of CO gas at the working electrode in the OTTLE cell and a Pt−CO stretch at 2103 cm^{-1} in the IR spectra. It is noteworthy that related $[Ru^0(CO)(THF)(bpy)]_n$ (ν(CO) at 1873 cm^{-1}) could be reduced reversibly to $[Ru^0(CO)$

dx.doi.org/10.1021/ic402146t | Inorg. Chem. 2014, 53, 1382−1396

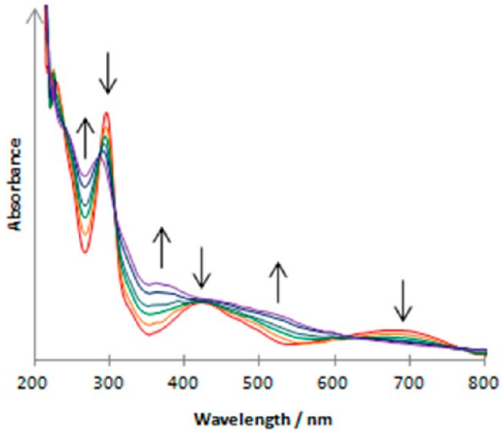

Figure 13. UV−vis spectroelectrochemistry showing the reduction of $[Os^{II}(CO)\ (bpy)Cl_3]^-$ to $[Os^0(CO)\ (THF)(bpy)]_n$ in THF at 293 K within an OTTLE cell.

$(THF)(bpy^{\bullet-})^-]_n$ (ν(CO) at 1845 cm^{-1}) showing the bifurcated $\pi^*\pi^*(bpy^{\bullet-})$ absorption at 522 and 552 nm. For comparison, IR monitoring of the reduction of $[Os^{II}(CO)\ (bpy)Cl_3]^-$ was carried out also in DMF and MeCN. The formation of a low-intensity broad ν(CO) band at 1856 cm^{-1} in MeCN and at 1853 cm^{-1} in dimethylformamide (DMF) (Supporting Information, Figures S4 and S5, respectively) suggests, similar to the case with THF, that in both solvents a linear Os(0) polymer chain is formed. Again, these experiments have revealed the unique position of the PrCN solvent already recognized in the cathodic behavior of related $[Os^{II}(CO)_2\ (bpy)Cl_2]$ (see above).

Cyclic Voltammetry of *trans*(Cl)-$[Os^{II}(CO)\ (PrCN)\ (bpy)Cl_2]$ in PrCN. From the spectroelectrochemical studies of *mer*-$[Os^{III}(CO)\ (bpy)Cl_3]$[35] it has been concluded that the solvent has a significant effect on the product formed on the reduction of $[Os^{II}(CO)\ (bpy)Cl_3]^-$ at RT. In THF, the $[Os^0(CO)\ (THF)(bpy)]_n$ polymer is observed; whereas, in PrCN the reduced species is probably $[Os^0(CO)\ (PrCN)(bpy)]$. The comparison of the spectroelectrochemistry of *trans*(Cl)-$[Os^{II}(CO)(PrCN)\ (bpy)Cl_2]$ and *mer*-$[Os^{III}(CO)\ (bpy)Cl_3]$[35]) is of interest as the former Os(II) complex has the butyronitrile ligand already precoordinated.

The cyclic voltammogram of $[Os^{II}(CO)\ (PrCN)\ (bpy)Cl_2]$ in PrCN at RT (Supporting Information, Figure S6) shows a reversible anodic wave at $E_{1/2}$ = +0.32 V corresponding to the Os^{II}/Os^{III} redox couple (eq 12).

$$[Os^{II}(CO)(PrCN)(bpy)Cl_2] \leftrightarrow [Os^{III}(CO)(PrCN)(bpy)Cl_2]^+ + e^- \quad (12)$$

In the cathodic region, a reversible couple is observed at $E_{1/2}$ = −1.87 V and is attributed to the bpy-based 1e⁻ reduction of $[Os^{II}(CO)(PrCN)\ (bpy)Cl_2]$ (eq 13). It lies at a very similar anodic potential to that of the $[Os^0(CO)(bpy)\ (PrCN)]/[Os^0(CO)(bpy^{\bullet-})\ (PrCN)]^-$ redox couple observed in the cyclic voltammogram of $[Os^{III}(CO)(bpy)Cl_3]$ in PrCN (Table 2). Therefore, it is expected that $[Os^0(CO)\ (bpy)(PrCN)]$, once formed (eq 14), becomes rapidly reduced to $[Os^0(CO)(bpy^{\bullet-})\ (PrCN)]^-$ (eq 8).

$$[Os^{II}(CO)(PrCN)(bpy)Cl_2] + e^- \leftrightarrow [Os^{II}(CO)(PrCN)(bpy^{\bullet-})Cl_2]^- \quad (13)$$

$$[Os^{II}(CO)(PrCN)(bpy^{\bullet-})Cl_2]^- + e^- \rightarrow [Os^0(CO)(PrCN)(bpy)] + 2Cl^- \quad (14)$$

Although the secondary reduction of $[Os^0(CO)\ (PrCN)(bpy)]$ to $[Os^0(CO)\ (bpy^{\bullet-})(PrCN)]^-$ cannot be indentified easily in the cyclic voltammogram of $[Os(CO)\ (PrCN)(bpy)Cl_2]$, IR spectroelectrochemistry at variable temperature is a suitable tool to determine whether the Os(0) species do form.

Spectroelectrochemistry of $[Os^{II}(CO)\ (PrCN)(bpy)Cl_2]$ in PrCN at 293 K. The IR spectrum of $[Os(CO)\ (PrCN)(bpy)Cl_2]$ (Figure 14) shows a ν(CO) stretch at 1932 cm^{-1}. Upon the reduction, this absorption band is shifted to 1895 cm^{-1}, and a ν(CN) stretch appears instantly at 2183 cm^{-1}, corresponding to the formation of $[Os(CO)\ (PrCN)(bpy^{\bullet-})]^-$ (eqs 13, 14). Parallel UV−vis monitoring of the cathodic path revealed replacement of the absorption bands of $[Os(CO)(PrCN)(bpy)Cl_2]$ at 298, 395, and 550 nm (see Supporting Information, Figure S7) by a new set with absorption maxima at 352, 386, and 490/523 nm belonging to $[Os^0(CO)\ (PrCN)(bpy^{\bullet-})]^-$ (see Figure 7). Reverse oxidation of this species resulted in the IR ν(CO) and ν(CN) absorptions shifting to 1927 cm^{-1} and 2194 cm^{-1}, respectively, as $[Os^0(CO)\ (PrCN)(bpy)]$ was produced. The corresponding UV−vis absorption spectrum exhibits bands at 289, 412, and 590 nm (Supporting Information, Figure S8). In theory it should be possible to reduce $[Os^{II}(CO)\ (PrCN)(bpy)Cl_2]$ first to $[Os^0(CO)\ (PrCN)(bpy)]$ and concomitantly to $[Os^0(CO)\ (PrCN)(bpy^{\bullet-})]^-$; however, the corresponding cathodic waves are strongly overlapping ($\Delta E_{1/2}$ = 0.01 V, Table 2), which prevents the resolution of the individual steps.

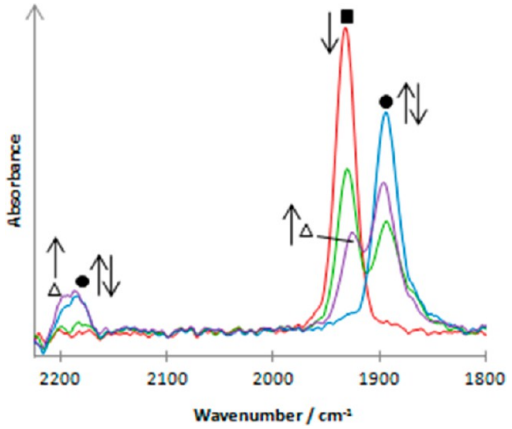

Figure 14. IR spectroelectrochemistry of $[Os^{II}(CO)\ (PrCN)(bpy)Cl_2]$ (■) showing the reduction to $[Os^0(CO)\ (PrCN)(bpy^{\bullet-})]^-$ (●) and subsequent reoxidation to $[Os^0(CO)\ (PrCN)(bpy)]$ (△) in PrCN at 293 K within an OTTLE cell.

Spectroelectrochemistry of $[Os^{II}(CO)\ (PrCN)(bpy)Cl_2]$ in PrCN at 213 K. The 1e⁻ reduction of $[Os^{II}(CO)\ (PrCN)(bpy)Cl_2]$ in PrCN at 213 K results in the shift of the diagnostic IR ν(CO) band from 1931 cm^{-1} to 1895 cm^{-1} (Figure 15). The latter wavenumber is attributed to the primary reduction product, $[Os^{II}(CO)\ (PrCN)(bpy^{\bullet-})Cl_2]^-$ (eq 13). This species remained stable up to 253 K. In the visible spectral region the characteristic bifurcated $\pi^*\pi^*(bpy^{\bullet-})$ absorption band of the latter radical complex was observed at 505/540 nm (see Supporting Information, Figure S9), that is, at a slightly lower energy than recorded for $[Os^0(CO)\ (PrCN)(bpy^{\bullet-})]^-$ (Table 3) formed at ambient temperature (ca. 293 K). The IR spectrum

dx.doi.org/10.1021/ic402146t | Inorg. Chem. 2014, 53, 1382−1396

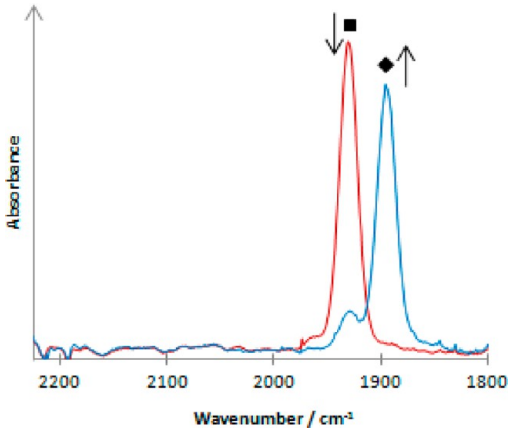

Figure 15. IR spectroelectrochemistry of $[Os^{II}(CO)(PrCN)(bpy)Cl_2]$ (■) showing the reduction to $[Os^{II}(CO)(PrCN)(bpy^{\bullet-})Cl_2]^-$ (◆) in PrCN at 213 K within an OTTLE cell.

of the Os(0) reduction product shows the ν(CO) band at 1895 cm^{-1} and the ν(CN) band at 2183 cm^{-1} (Figure 5). Importantly, the ν(CN) band below 2200 cm^{-1} is absent in the IR spectrum $[Os^{II}(CO)(PrCN)(bpy^{\bullet-})Cl_2]^-$ (Figure 15), proving that the reduction products formed at 293 and 213 K are different. The identical ν(CO) wavenumbers reveal the same degree of the Os-to-CO π-back-donation from the π-delocalized $Os^{II}Cl_2$ and reduced Os(0) centers.

Spectroelectrochemistry of $[Os^{II}(CO)(PrCN)(bpy)Cl_2]$ in THF at 293 K. IR monitoring of the reduction path of $[Os^{II}(CO)(PrCN)(bpy)Cl_2]$ (ν(CO) at 1934 cm^{-1}) in THF at 293 K revealed an intermediate absorbing at 1896 cm^{-1} (Figure 16). This monocarbonyl complex is assigned tentatively as

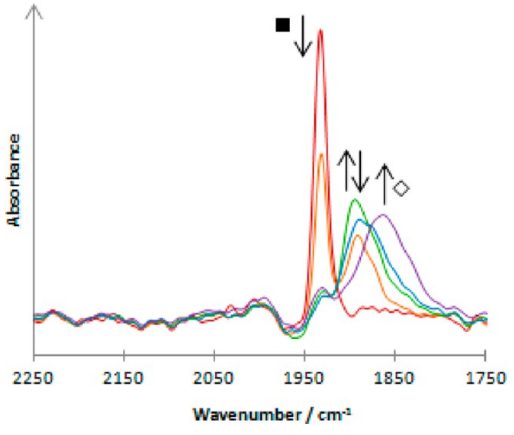

Figure 16. IR spectroelectrochemistry of $[Os^{II}(CO)(PrCN)(bpy)Cl_2]$ (■) showing the reduction to $[Os^{0}(CO)(THF)(bpy)]_n$ (◇) in THF at 293 K within an OTTLE cell.

$[Os^{II}(CO)(PrCN)(bpy^{\bullet-})Cl_2]^-$, slowly converting in THF to an ultimate Os(0) product with a broad ν(CO) band at 1860 cm^{-1}. No ν(CN) band is perceptible below 2200 cm^{-1}, excluding the PrCN coordination at the Os(0) center. The almost-identical ν(CO) wavenumbers and bandwidth seen for the $2e^-$ reduction of $[Os^{II}(CO)(bpy)Cl_3]^-$ (Figure 12) and $[Os^{II}(CO)(PrCN)(bpy)Cl_2]$ in THF indicate that in both cases the THF-substituted polymer $[Os^{0}(CO)(THF)(bpy)]_n$ is formed. This result differs from the reduction of $[Ru^{II}(CO)(PrCN)(bpy)Cl_2]$ in THF, where a ν(CN) stretch appeared below 2200 cm^{-1} as $[Ru^{0}(CO)(PrCN)(bpy)]$ was first produced.[3]

In summary, cyclic voltammetry and spectroelectrochemistry have shown that the electrolyte solution has a significant effect on the electrochemical behavior of the two osmium monocarbonyl complexes $[Os^{III}(CO)(bpy)Cl_3]$ and $[Os^{II}(CO)(PrCN)(bpy)Cl_2]$. In THF at ca. 293 K, the bpy-localized $1e^-$ reduction of these complexes triggers the formation of the polymer species $[Os^{0}(CO)(THF)(bpy)]_n$ characterized by a broad, low intensity ν(CO) band in the IR spectrum. In PrCN, the same reduction results in the appearance of a sharper, more intense, ν(CO) band at a much larger wavenumber, accompanied by a ν(CN) stretch below 2200 cm^{-1} resulting from PrCN coordination at the Os(0) center in $[Os^{0}(CO)(PrCN)(bpy)]$ and its bpy-reduced form. DFT calculations have been carried out to support this assignment (see the next section). The reduction paths of the two monocarbonyl complexes under study are presented in Scheme 1.

Scheme 1. A Simplified Redox Path of the Title Complexes in PrCN and THF[a]

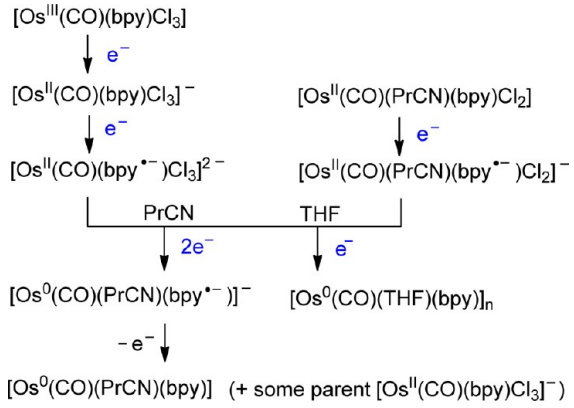

[a]The substitution of the chloride ligands in the $Os^{II}(bpy^{\bullet-})$ complexes by the coordinating solvent (an electrochemical–chemical–electrochemical route in PrCN) can be prevented at sufficiently low temperatures.

Similar differences in the reduction paths were observed for the related dicarbonyl complex $[Os^{II}(CO)_2(bpy)Cl_2]$ in PrCN and in THF/MeCN. In the latter solvents, an insoluble polymeric film, $[\{Os^{0}(CO)_2(bpy)\}]_n$, is deposited on the working electrode, characterized by broad and low-intensity ν(CO) bands at 1959, 1900, and 1868 cm^{-1}. In contrast, sharp and intense ν(CO) bands at 1940 and1855 cm^{-1} and a ν(CN) stretch at 2176 cm^{-1} are seen in PrCN.[14] Comparison with the bpy-based reductions of $[Os^{II}(CO)(bpy)Cl_3]^-$ and $[Os^{II}(CO)(PrCN)(bpy)Cl_2]$ implies the formation of a PrCN-stabilized mononuclear species, $\{Os^{0}(CO)_2(PrCN)(bpy)\}$, having possibly a pyramidal structure. As a convincing example of a well-characterized mononuclear complex showing a very similar shift to a smaller ν(CN) wavenumber may serve $[Re(CO)_3(PrCN)(bpy)]^+$ and its $2e^-$-reduced form, $[Re(CO)_3(PrCN)(bpy)]^-$ that dominates in the PrCN solution over five-coordinate $[Re(CO)_3(bpy)]^-$.[14,39]

DFT Calculations of *mer*-$[Os^{III}(CO)(bpy)Cl_3]$ and *mer*-$[Os^{II}(CO)(bpy)Cl_3]^-$. DFT calculations were carried out on *mer*-$[Os^{III}(CO)(bpy)Cl_3]$, *mer*-$[Os^{II}(CO)(bpy)Cl_3]^-$, and on the hypothetical fac isomers of both complexes (Supporting Information, Figure S10 and Table S3). The geometry optimizations and the TD-DFT calculations were performed in MeCN, to deal with the negatively charged species.

dx.doi.org/10.1021/ic402146t | Inorg. Chem. 2014, 53, 1382–1396

The complex *fac*-[Os^{III}(CO) (bpy)Cl_3] was calculated to be more stable than the mer isomer by only ~2 kcal mol^{-1}, while the *mer*-[Os^{II}(CO) (bpy)Cl_3]$^-$ complex was more stable by ~1 kcal mol^{-1} than the fac isomer. Only the mer isomer has been experimentally observed for Os(III), and the electrochemically reversible reduction to the Os(II) state (Figures 2–4) hardly supports any isomerization triggered by electron transfer.

The α frontier orbitals of $5d^5$ *mer*-[Os^{III}(CO) (bpy)Cl_3] are shown in Figure 17. The α-HOMO is a t_{2g} orbital, with 61.8%

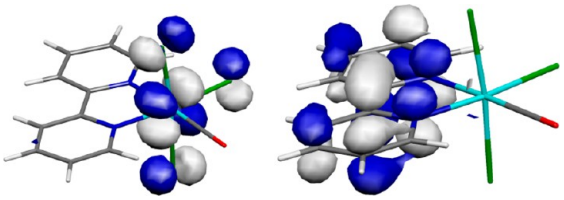

Figure 17. The α-HOMO and LUMO of *mer*-[Os^{III}(CO) (bpy)Cl_3].

localization on Os and 20.4% on Cl; whereas, the LUMO is 88.1% on the bpy ligand. The first reduction leads to the occupation of the β LUMO, also concentrated on the metal as the α-HOMO, while the second one results in occupying the α LUMO (also the LUMO of *mer*-[Os^{II}(CO) (bpy)Cl_3]$^-$ as expected).

The nature of the frontier orbitals is in agreement with the large shift ($\Delta\nu$(CO) = 111 cm^{-1}) determined from IR spectroelectrochemistry, implying that reduction of *mer*-[Os^{III}(CO) (bpy)Cl_3] takes place at the metal center, and the reduction of the resulting anion *mer*-[Os^{II}(CO) (bpy)Cl_3]$^-$, associated with a much smaller shift ($\Delta\nu$(CO) = 37 cm^{-1}), occurs on the coordinated bpy (see above).

The TD-DFT calculated electronic absorption spectrum of *mer*-[Os^{II}(CO) (bpy)Cl_3]$^-$ displays bands at 710, 554, and 441 nm and an intense band at 294 nm with a shoulder at 265 nm, in good agreement with the experimental UV–vis absorption spectrum exhibiting a strong band at 299 nm and less intense bands at 420 nm (with a shoulder at 465 nm) and 658 nm (Figure 18). The calculated electronic transitions (Supporting Information, Table S4 and Figure S11) allow these bands to be assigned as MLCT from π^*(Os–Cl) to π^*(bpy), with an interligand contribution from p_π(Cl) to π^*(bpy) in the highest energy band shown, as can clearly be seen in the plots (Figure 18; blue indicating a decrease in electron density and yellow an increase).

DFT Calculations of [Os(CO)(MeCN)(bpy)Cl_2]. DFT calculations showed that the energy of *trans*(Cl)-[Os(CO)-(MeCN) (bpy)Cl_2] is the highest of the possible isomers of this complex, but there was only a difference of ~1 kcal mol^{-1} between the highest and lowest energy isomer (gas phase). Geometries and relative energies of several isomers of [Os-(CO)(MeCN) (bpy)Cl_2] are available in the Supporting Information (Figure S12, Table S5). The trans isomer is experimentally observed, while for the analogous ruthenium complex it is the cis isomer that is seen.[3,17]

The calculated frontier orbitals of *trans*-[Os(CO) (MeCN) (bpy)Cl_2] reveal that the participation of the chlorine atoms in the t_{2g} orbitals of Os(II) is much higher than it is in other similar complexes. The HOMO and HOMO-1 spread over the osmium metal center (43.5 and 33.2%) and the coordinated chloride ligands (38.8 and 54.1%) so that these orbitals do not have a predominant d character and should be considered π^*(Os–Cl). The LUMO is essentially based on the bpy ligand (85.6% bpy), with only 7.0% Os d (Figure 19). This indicates that oxidation

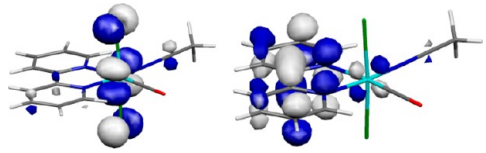

Figure 19. The HOMO and LUMO of *trans*-[Os(CO)(MeCN) (bpy)Cl_2].

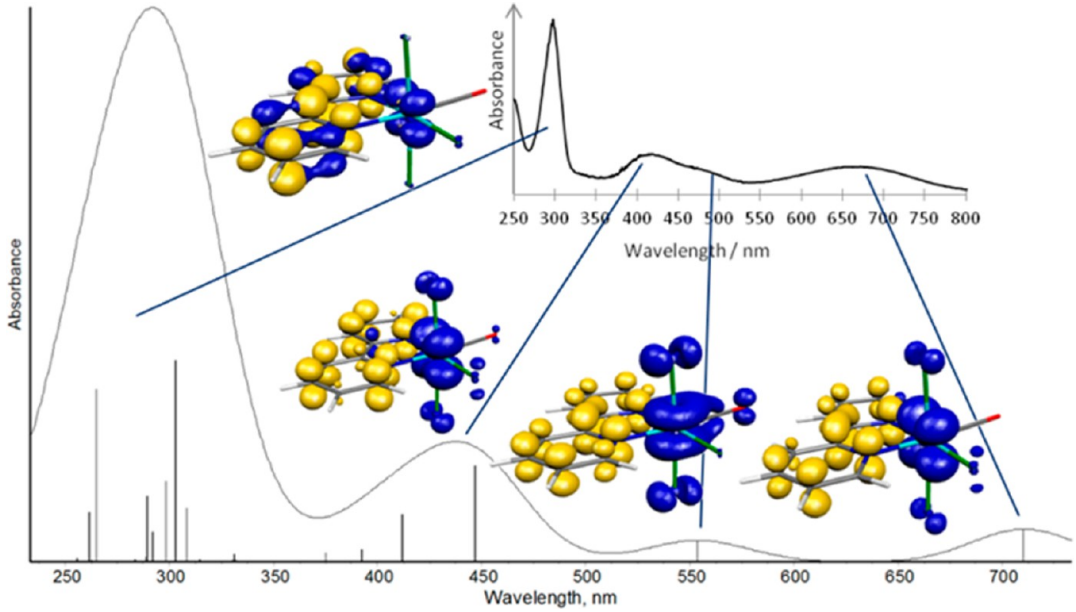

Figure 18. TD-DFT calculated electronic absorption spectrum of *mer*-[Os^{II}(CO) (bpy)Cl_3]$^-$ in MeCN. The vertical excitations correspond to data in Supporting Information, Table S4. Inset: the corresponding experimental spectrum in PrCN at 293 K (Figure 6).

dx.doi.org/10.1021/ic402146t | *Inorg. Chem.* 2014, 53, 1382–1396

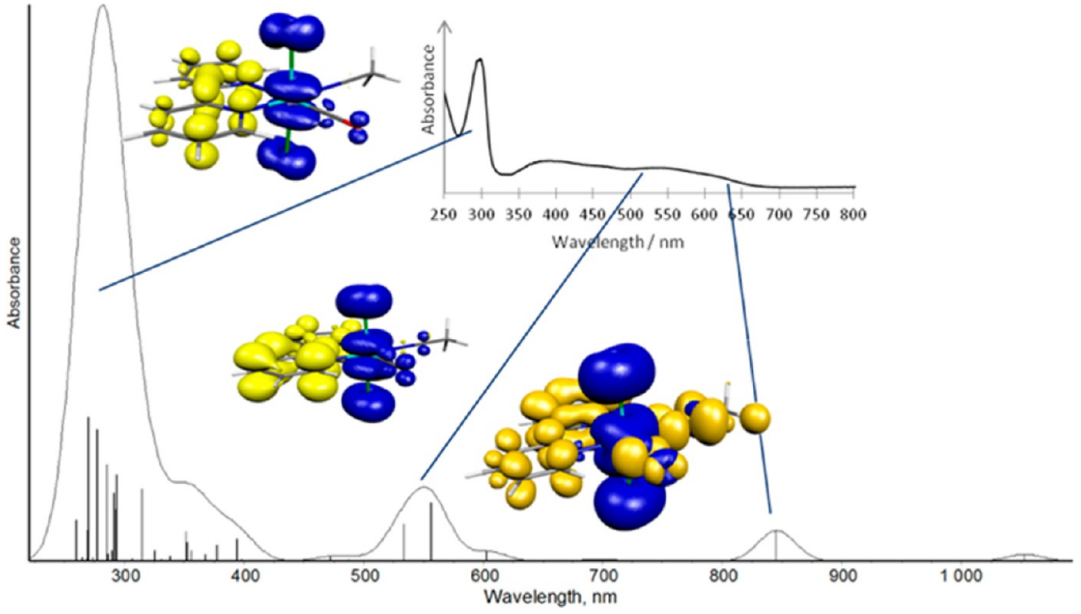

Figure 20. TD-DFT calculated electronic absorption spectrum of *trans*-[Os^{II}(CO) (MeCN) (bpy)Cl_2]. The vertical excitations correspond to data in Supporting Information, Table S6. Inset: the corresponding experimental spectrum in PrCN, 293 K (Supporting Information, Figure S7).

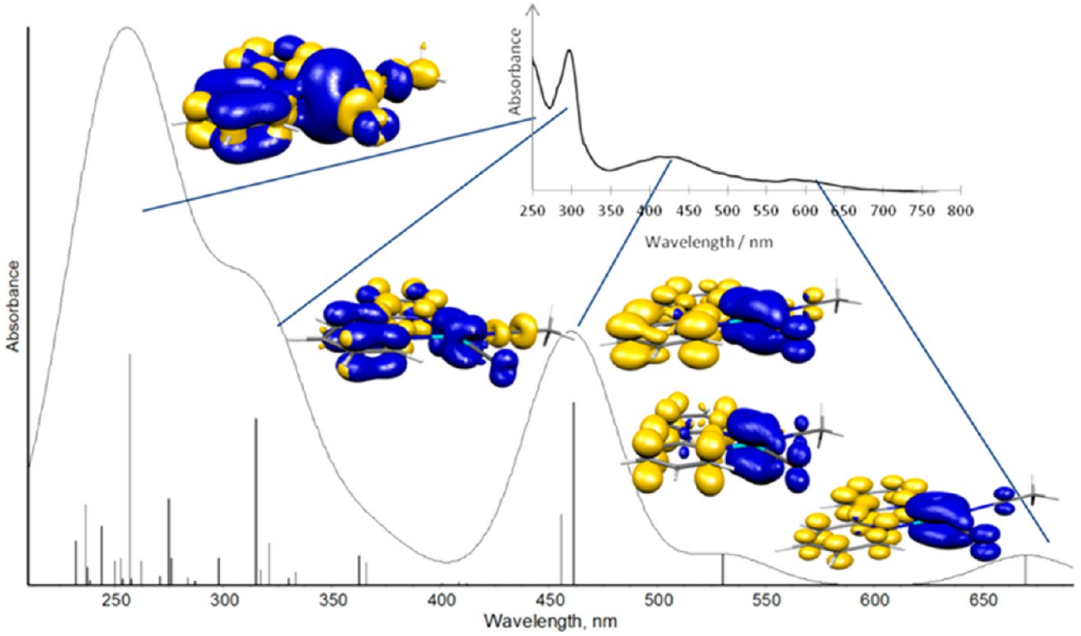

Figure 21. TD-DFT calculated electronic absorption spectrum for [Os^0(CO) (MeCN)(bpy)]. The vertical excitations correspond to data in Supporting Information, Table S8. Inset: the corresponding experimental spectrum of [Os^0(CO) (PrCN)(bpy)] in PrCN at 293 K (Supporting Information, Figure S8).

leads to the strengthening of the Os−Cl bond, as $1e^-$ is removed from the π^*(Os−Cl) orbital, while the reduction takes place on the bpy ligand, as happened with [Os^{II}(CO) (bpy)Cl_3]$^-$.

The TD-DFT calculated electronic absorption spectrum of *trans*-[Os^{II}(CO) (MeCN) (bpy)Cl_2] (Figure 20, Supporting Information, Table S6 and Figure S13) displays absorptions at 549 and 846 nm and an intense absorption at 283 nm with a shoulder at a slightly higher wavelength. Higher energy bands were not calculated. These electronic transitions mainly start from the HOMO, HOMO-1, and HOMO-2, all being π^*(Os−Cl), and HOMO-5, which is π(Os−Cl). The excitations end at the LUMO, LUMO+2, and LUMO+4, all being π^*(bpy) orbitals. The transitions can therefore be assigned as a π/π^*(Os−Cl)-to-π^*(bpy) charge transfer, as can clearly be seen in the plots where blue indicates a decrease in electron density and yellow indicates an increase (Figure 20). The calculated IR spectrum of *trans*-[Os^{II}(CO) (MeCN) (bpy)Cl_2] was shown to have a ν(CO) stretch at 1950 cm^{-1} and a ν(CN) stretch at 2258 cm^{-1}. The ν(CO) stretch is in a relatively good agreement with that observed experimentally in PrCN at 1932 cm^{-1}, but the ν(CN) stretch is obscured by the solvent band (see above).

The relatively good agreement between the experimental and calculated data described above indicates that this DFT

dx.doi.org/10.1021/ic402146t | *Inorg. Chem.* 2014, 53, 1382−1396

methodology is suitable to investigate these osmium complexes. Therefore, it has been applied to identify possible structures for the mononuclear species formed from the reduction of *mer*-$[Os^{II}(CO)(bpy)Cl_3]^-$ and *trans*(Cl)-$[Os^{II}(CO)(PrCN)(bpy)Cl_2]$ in PrCN, which were detected by their spectroscopic data. Experimental results showed that $[Os^0(CO)(PrCN)(bpy)]$ could not be an oligomer, as no ν(CN) peaks were observed for the coordination of PrCN at the terminal Os(I) centers.

DFT Calculations of Os(0) Mono- and Dinuclear Species. DFT calculations were carried out on the square-planar complexes $[Os(CO)(MeCN)(bpy)]^n$ (n = +1, 0, −1) with osmium in the −I, 0 and +I formal oxidation states (Supporting Information, Table S7), to compare with the experimental spectroscopic evidence that an Os(0) complex resulted from the multielectron reduction of *mer*-$[Os^{III}(CO)(bpy)Cl_3]$ and *trans*(Cl)-$[Os^{II}(CO)(PrCN)(bpy)Cl_2]$ in PrCN.

Comparison with experimental values for the ν(CO) and ν(CN) stretches of $[Os^0(CO)(PrCN)(bpy)]$ (1927 and 2194 cm^{-1}, respectively, Table 3) shows that the values calculated for $[Os^0(CO)(MeCN)(bpy)]$, 1884 and 2182 cm^{-1}, support the assignment of the mononuclear Os(0) species (Supporting Information, Figure S14). Calculated frequencies for the Os(I) complex are too high, while those obtained for Os(−I) are too low. The electronic absorption spectrum calculated for $[Os^0(CO)(MeCN)(bpy)]$ (Supporting Information, Table S8, Figure 21), with maxima at 670, 460, 256 nm and shoulders at 531 and 315 nm, is also in a good agreement with the experimental UV−vis absorption spectrum of $[Os^0(CO)(PrCN)(bpy)]$. The plots indicate that the two lowest-energy transitions are π/π^*(Os−Cl)-to-π^*(bpy) charge transfers (blue indicates a decrease in electron density and yellow indicates an increase), while the higher-energy ones have a considerable intraligand (IL) (CO and bpy) character (see also Supporting Information, Table S8 and Figure S15).

DFT calculations were also carried out for two other possible structures, square-pyramidal $[Os(CO)(bpy)(MeCN)_2]$ and the Os−Os bound dimer $[Os(CO)(MeCN)_2(bpy)]_2$ (Supporting Information, Figures S16 and S17). However, their IR spectra showed poor agreement with the experimental data for $[Os(CO)(PrCN)(bpy)]$ (Supporting Information, Table S9). The species observed on the reduction of *mer*-$[Os^{III}(CO)(bpy)Cl_3]$ and *trans*(Cl)-$[Os^{II}(CO)(PrCN)(bpy)Cl_2]$ in PrCN are therefore most likely to be $[Os^0(CO)(PrCN)(bpy)]$. It is possible, however, that the reduction of the dicarbonyl complex, *trans*(Cl)-$[Os^{II}(CO)_2(bpy)Cl_2]$,[4] leads to a square-pyramidal or pseudo-octahedral Os(0) species with PrCN coordinated in the axial position(s), similar to *fac*-$[Re(CO)_3(PrCN)(bpy)]^-$.[5] X-ray structural analyses of the Os(0) species remain a challenge.

Catalytic CO_2 Reduction with $[Os^{III}(CO)(bpy)Cl_3]$ in PrCN. It was shown that the reduction of $[Os^{II}(CO)(bpy)Cl_3]^-$ and $[Os^{II}(CO)(PrCN)(bpy)Cl_2]$ in PrCN does not lead to formation of poly(Os−Os) chains but to a solvent-stabilized mononuclear complex, $[Os^0(CO)(PrCN)(bpy)]$. Preliminary experiments to investigate the catalytic behavior of the bpy-reduced species $[Os^0(CO)(PrCN)(bpy^{\bullet-})]^-$ toward CO_2 reduction have been carried out.

IR spectroelectrochemistry of parent $[Os^{III}(CO)(bpy)Cl_3]$ in PrCN and in the presence of CO_2 showed the appearance of a number of small ν(CO) bands between 1900 and 2100 cm^{-1} upon the reduction of $[Os^{II}(CO)(bpy)Cl_3]^-$ (Figure 22) accompanied by ν(CO) and ν(CN) bands at 1893 cm^{-1} and 2183 cm^{-1}, respectively, corresponding to $[Os(CO)(PrCN)(bpy^{\bullet-})]^-$. The $^{13}CO_2$ satellite peak is seen to decrease as

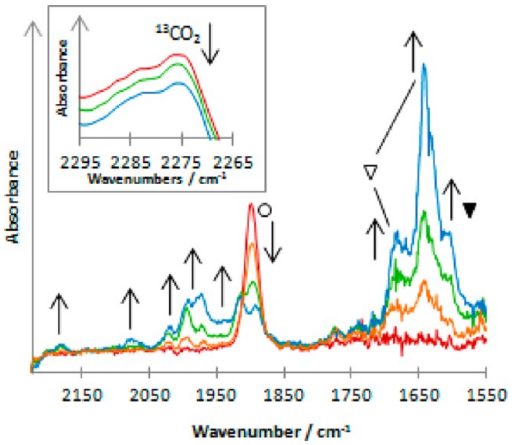

Figure 22. IR spectral changes accompanying the reduction of $[Os^{II}(CO)(bpy)Cl_3]^-$ (○) in PrCN saturated with CO_2. Formation of HCO_3^- (▽) and $HCOO^-$ (▲) was observed.

catalysis occurs. Absorption peaks at 1685 and 1642 cm^{-1} indicate the presence of HCO_3^-, and a peak at 1604 cm^{-1} corresponds to the production of formate.[40] Formation of CO gas was observed at the working electrode. This behavior is consistent with the cyclic voltammogram of $[Os^{III}(CO)(bpy)Cl_3]$ in PrCN saturated with CO_2 (Supporting Information, Figure S18). The catalytic current starts to rise directly beyond the cathodic wave of $[Os^{II}(CO)(bpy)Cl_3]^-$ where the catalyst $[Os^0(CO)(PrCN)(bpy^{\bullet-})]^-$ is generated (eqs 6 and 7).

Catalytic CO_2 Reduction with $[Os^{II}(CO)(PrCN)(bpy)Cl_2]$ in PrCN. The catalytic reduction of CO_2 in PrCN differs when the catalyst precursor is $[Os^{II}(CO)(PrCN)(bpy)Cl_2]$ rather than $[Os^{III}(CO)(bpy)Cl_3]$. As $[Os^{II}(CO)(PrCN)(bpy)Cl_2]$ is reduced, a range of unassigned ν(CO) stretches appear between 1850 and 2050 cm^{-1}. $[Os(CO)(PrCN)(bpy^{\bullet-})]^-$ is also observed by ν(CO) and ν(CN) bands at 1894 cm^{-1} and 2185 cm^{-1}, respectively (Figure 23).

The dominant CO_2 reduction product observed with IR spectroscopy was formate, absorbing at 1606 cm^{-1}. CO gas was again developing at the working electrode. Smaller carbonyl bands at 1688 and 1643 cm^{-1} indicate the presence of bicarbonate.[40]

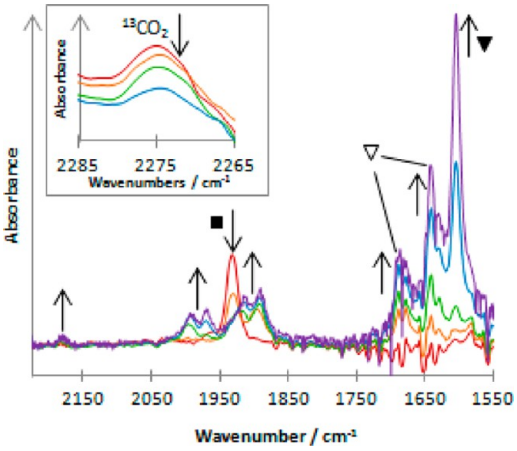

Figure 23. IR spectral changes accompanying the reduction of $[Os^{II}(CO)(PrCN)(bpy)Cl_2]$ (■) in PrCN saturated with CO_2. Formation of HCO_3^- (▽) and $HCOO^-$ (▼) was observed.

dx.doi.org/10.1021/ic402146t | *Inorg. Chem.* 2014, 53, 1382−1396

Catalytic CO_2 Reduction with $[Os^{III}(CO)(bpy)Cl_3]$ in THF. IR spectroelectrochemistry was also carried out in THF saturated with CO_2 to observe the catalytic behavior of the Os(0) polymers. Reduction of $[Os^{II}(CO)(bpy)Cl_3]^-$ led to the appearance of a small band at 2067 cm^{-1}, while the ν(CO) stretch of $[Os^0(CO)(THF)(bpy)]_n$ at 1860 cm^{-1} was not observed (Figure 24). The $^{13}CO_2$ satellite peak decreases as

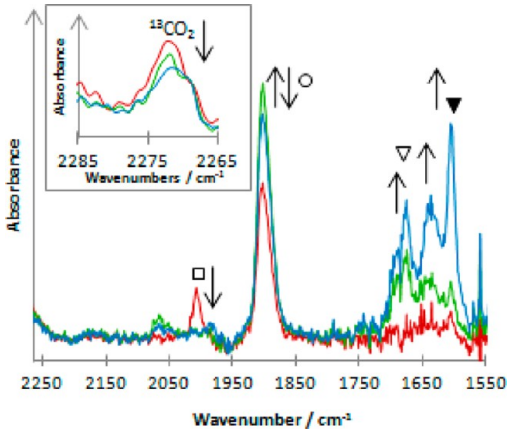

Figure 24. IR spectral changes accompanying the conversion of remaining $[Os^{III}(CO)(bpy)Cl_3]$ (□) to $[Os^{II}(CO)(bpy)Cl_3]^-$ (○), and subsequent reduction of the latter anion in THF saturated with CO_2. Formation of HCO_3^- (▽) and $HCOO^-$ (▼) was observed.

reduction occurs. Rapid appearance of absorption bands at 1678, 1642, and 1605 cm^{-1} reveals the formation of HCO_3^- and $HCOO^-$.[40] Bubbles were seen forming on the working electrode, indicating that CO is produced. This suggests that CO_2 coordination itself is capable of converting some of the $[Os^0(CO)(THF)(bpy)]_n$ polymer into catalytically active $Os^0(bpy^{\bullet-})$ fragments. Conventional cyclic voltammetry (Supporting Information, Figure S19), however, documents that the real onset of efficient catalytic reduction of CO_2 starts more negatively (in contrast to the situation in PrCN, Supporting Information, Figure S18), that is, in the potential region where $[Os^0(CO)(THF)(bpy)]_n$ undergoes the bpy-localized reduction (Figure 4).

The different electrocatalytic behavior of $[Os(CO)(bpy)Cl_3]$ in PrCN and THF nicely reflects the different nature of the catalytically active Os(0) species formed in these solvents. It remains unanswered, however, whether the true catalyst in THF has still the likely polymeric structure as formed in the absence of CO_2.

CONCLUSIONS

Cyclic voltammetry and in situ IR and UV−vis spectroelectrochemical monitoring at variable temperature have shown that the Os(0) products formed upon stepwise reduction of the monocarbonyl complexes $[Os^{III}(CO)(bpy)Cl_3]$ and $[Os^{II}(CO)(PrCN)(bpy)Cl_2]$ are strongly dependent on the solvent used. While coordinating butyronitrile PrCN stabilizes soluble mononuclear species, a polymer chain with different redox and spectroscopic properties is formed in THF and also in MeCN and DMF. DFT and TD-DFT calculations support the existence of planar $[Os^0(CO)(PrCN)(bpy)]$ that is also stable in the reduced state $[Os^0(CO)(PrCN)(bpy^{\bullet-})]^-$ formed directly from $[Os^{II}(CO)(bpy^{\bullet-})Cl_3]^{2-}$ or $[Os^{II}(CO)(PrCN)(bpy^{\bullet-})Cl_2]^-$ at RT (293 K). The latter electron-rich radicals are stable only at low temperature (213 K) in the presence of a high excess of Cl^- ions, unlike the analogous but much more reactive Ru(II) species. The key signature of the soluble $Os^0(bpy)$ and $Os^0(bpy^{\bullet-})$ *monocarbonyl* products is the ν(CN) stretch of the PrCN ligand appearing below 2200 cm^{-1}, similar to the electronically close complex $[Re(CO)_3(PrCN)(bpy)]^-$. Importantly, the solvent control of solubility applies also to $Os^0(bpy)$ and $Os^0(bpy^{\bullet-})$ *dicarbonyl* complexes known to form insoluble polymer chains in THF and MeCN but existing as soluble compounds in PrCN; in this solvent they also feature the characteristic ν(CN) stretch omitted in the previous reports. Preliminary investigations indicate that $[Os^0(CO)(PrCN)(bpy^{\bullet-})]^-$ is capable of catalytically reducing CO_2 to CO, where the parent complex is $[Os^{III}(CO)(bpy)Cl_3]$, and to both CO and formate for $[Os^{II}(CO)(PrCN)(bpy)Cl_2]$.

ASSOCIATED CONTENT

Supporting Information

X-ray crystallographic data for the complexes *mer*-$[Os(bpy)Cl_3(CH_3OH)]\cdot CH_3OH$ and *mer*-$[Os(CO)(bpy)Cl_3]$ in CIF format. Thermal ellipsoid view and crystal data for *mer*-$[Os(bpy)Cl_3(CH_3OH)]\cdot CH_3OH$. CV of *mer*-$[Os(CO)(bpy)Cl_3]$ in PrCN (two cathodic cycles combined with delayed potential sweep) and in THF at T = 293 K. IR monitoring of the reduction of *mer*-$[Os^{II}(CO)(bpy)Cl_3]^-$ in MeCN and DMF at T = 293 K. CV and UV−vis absorption spectrum of *trans*(Cl)-$[Os^{II}(CO)(bpy)(PrCN)Cl_2]$ in PrCN at T = 293 K. UV−vis absorption spectra of $[Os^0(CO)(PrCN)(bpy)]$ in PrCN at T = 293 K and *trans*(Cl)-$[Os^{II}(CO)(PrCN)(bpy^{\bullet-})Cl_2]^-$ at T = 213 K in PrCN/excess Cl^-. Optimized structures and relative energies of the mer and fac isomers of $[Os(CO)(bpy)Cl_3]$ and $[Os(CO)(bpy)Cl_3]^-$ calculated with DFT. Electronic transitions in *mer*-$[Os^{II}(CO)(bpy)Cl_3]^-$ calculated with TD-DFT. Optimized structures and relative energies of the trans(Cl) and two *cis*(Cl) isomers of $[Os(CO)(MeCN)(bpy)Cl_2]$ calculated with DFT. Electronic transitions for *trans*(Cl)-$[Os^{II}(CO)(MeCN)(bpy)Cl_2]$ calculated with TD-DFT. Optimized structure of $[Os^0(CO)(MeCN)(bpy)]$ calculated with DFT. Electronic transitions for $[Os^0(CO)(MeCN)(bpy)]$ calculated with TD-DFT. Optimized structures and IR ν(CN) and ν(CO) wavenumbers of $[Os^0(CO)(MeCN)_2(bpy)]$ and $[Os^0(CO)(MeCN)_2(bpy)]_2$ calculated with DFT. CV of *mer*-$[Os(CO)(bpy)Cl_3]$ in PrCN and THF saturated with CO_2. This material is available free of charge via the Internet at http://pubs.acs.org.

AUTHOR INFORMATION

Corresponding Author

*E-mail: f.hartl@reading.ac.uk. Tel.: +44-118 378 7695. Fax: +44 118 378 6331.

Notes

The authors declare no competing financial interest.

ACKNOWLEDGMENTS

This work was partly conducted within COST D29. F.H. and J.T. acknowledge the University of Reading for financial support (a start-up grant). Dr. Q. Zeng (Reading) helped with some of the low-temperature spectroelectrochemical experiments. Mr. H. Luyten (Purmerend, The Netherlands) is thanked for the technical maintenance of the spectroelectrochemical cells. M.H. thanks Mrs. Taina Nivajärvi from University of Eastern Finland for her valuable work with the synthesis and elemental analysis of the Os complexes. M.J.C. thanks Fundação para a Ciência e

Tecnologia, Portugal, for financial support (PEst-OE/QUI/UI0216/2013) and D. Vila-Viçosa for the help with plotting EDD maps from ADF results.

REFERENCES

(1) (a) Chardon-Noblat, S.; Deronzier, A.; Ziessel, R. *Collect. Czech. Chem. Commun.* **2001**, *66*, 207−227. (b) Chauvin, J.; Lafolet, F.; Chardon-Noblat, S.; Deronzier, A.; Jakonen, M.; Haukka, M. *Chem.—Eur. J.* **2011**, *17*, 4313−4322.

(2) Collomb-Dunand-Sauthier, M. N.; Deronzier, A.; Ziessel, R. *Inorg. Chem.* **1994**, *33*, 2961−2967.

(3) Hartl, F.; Renfrew, A. K.; Lafolet, F.; Mahabiersing, T.; Calhorda, M. J.; Chardon-Noblat, S.; Haukka, M.; Deronzier, A. *Inorg. Chem.* **2009**, *48*, 8233−8244.

(4) Hartl, F.; Mahabiersing, T.; Chardon-Noblat, S.; Da Costa, P.; Deronzier, A. *Inorg. Chem.* **2004**, *43*, 7250−7258.

(5) Panteli, E.; Hartl, F. Unpublished results. A ν(CN) band was observed at 2176 cm^{-1} for $[Re^0(CO)_3(bpy)(PrCN)]^-$ produced from $2e^-$ reduction of $[Re^I(CO)_3(bpy)(Otf)]$ in PrCN. University of Reading, U.K., 2011.

(6) Chardon-Noblat, S.; Deronzier, A.; Zsoldos, D.; Ziessel, R.; Haukka, M.; Pakkanen, T.; Venäläinen, T. *J. Chem. Soc., Dalton Trans.* **1996**, 2581−2583.

(7) Masciocchi, N.; Sironi, A.; Chardon-Noblat, S.; Deronzier, A. *Organometallics* **2002**, *21*, 4009−4012.

(8) Gerbaud, G.; Mouesca, J.-M.; Hediger, S.; Chardon-Noblat, S.; Lafolet, F.; Deronzier, A.; Bardet, M. *Phys. Chem. Chem. Phys.* **2010**, *12*, 15428−15435.

(9) Niskanen, M.; Hirva, P.; Haukka, M. *Phys. Chem. Chem. Phys.* **2010**, *12*, 9777−9782.

(10) Masciocchi, N.; Moret, M.; Cairati, P.; Ragaini, F.; Sironi, A. *J. Chem. Soc., Dalton Trans.* **1993**, 471−475.

(11) Myllynen, S.; Wasberg, M. *Electrochem. Commun.* **2009**, *11*, 1453−1456.

(12) (a) Chardon-Noblat, S.; Cripps, G. H.; Deronzier, A.; Field, J. S.; Gouws, S.; Haines, R. J.; Southway, F. *Organometallics* **2001**, *20*, 1668−1675. (b) Collomb-Dunand-Sauthier, M. N.; Deronzier, A.; Ziessel, R. *J. Chem. Soc., Chem. Commun.* **1994**, 189−191. (c) Chardon-Noblat, S.; Deronzier, A.; Ziessel, R.; Zsoldos, D. *J. Electroanal. Chem.* **1998**, *444*, 253−260.

(13) (a) Arai, T.; Sato, S.; Uemura, K.; Morikawa, T.; Kajino, T.; Motohiro, T. *Chem. Commun.* **2010**, *46*, 6944−6946. (b) Sato, S.; Arai, T.; Morikawa, T.; Uemura, K.; Suzuki, T. M.; Tanaka, H.; Kajino, T. *J. Am. Chem. Soc.* **2011**, *133*, 15240−15243. (c) Arai, T.; Tajima, S.; Sato, S.; Uemura, K.; Morikawa, T.; Kajino, T. *Chem. Commun.* **2011**, *47*, 12664−12666.

(14) Maroulis, A.; Hartl, F. University of Reading, U.K., 2011. Unpublished results.

(15) Chardon-Noblat, S.; Deronzier, A.; Hartl, F.; van Slageren, J.; Mahabiersing, T. *Eur. J. Inorg. Chem.* **2001**, 613−617.

(16) Eskelinen, E.; Da Costa, P.; Haukka, M. *J. Electroanal. Chem.* **2005**, *579*, 257−265.

(17) Chardon-Noblat, S.; Da Costa, P.; Deronzier, A.; Mahabiersing, T.; Hartl, F. *Eur. J. Inorg. Chem.* **2002**, 2850−2856.

(18) Duisenberg, A. J. M.; Kroon-Batenburg, L. M. J.; Schreurs, A. M. M. *J. Appl. Crystallogr.* **2003**, *36*, 220−229.

(19) Sheldrick, G. M. *Acta Crystallogr., Sect. A* **2008**, *64*, 112−122.

(20) Sheldrick, G. M. *SADABS—Bruker AXS Scaling and Absorption Correction*; Bruker AXS: Madison, Wisconsin, 2008.

(21) (a) Krejčík, M.; Danek, M.; Hartl, F. *J. Electroanal. Chem.* **1991**, *317*, 179−187. (b) Hartl, F.; Luyten, H.; Nieuwenhuis, H. A.; Schoemaker, G. C. *Appl. Spectrosc.* **1994**, *48*, 1522−1528. (c) Mahabiersing, T.; Luyten, H.; Nieuwendam, R. C.; Hartl, F. *Collect. Czech. Chem. Commun.* **2003**, *68*, 1687−1709.

(22) Parr, R. G.; Yang, W. *Density Functional Theory of Atoms and Molecules*; Oxford University Press: New York, 1989.

(23) (a) te Velde, G.; Bickelhaupt, F. M.; van Gisbergen, S. J. A.; Guerra, C. F.; Baerends, E. J.; Snijders, J. G.; Ziegler, T. *J. Comput. Chem.* **2001**, *22*, 931−967. (b) Guerra, C. F.; Snijders, J. G.; te Velde, G.; Baerends, E. J. *Theor. Chem. Acc.* **1998**, *99*, 391−403. (c) ADF2009, SCM, Theoretical Chemistry; Vrije Universiteit: Amsterdam, The Netherlands. http://www.scm.com/. (Accessed March 1, 2009).

(24) (a) Versluis, L.; Ziegler, T. *J. Chem. Phys.* **1988**, *88*, 322−328. (b) Fan, L. Y.; Ziegler, T. *J. Chem. Phys.* **1991**, *95*, 7401−7408.

(25) Vosko, S. H.; Wilk, L.; Nusair, M. *Can. J. Phys.* **1980**, *58*, 1200−1211.

(26) (a) Becke, A. D. *Phys. Rev. A* **1988**, *38*, 3098−3100. (b) Perdew, J. P. *Phys. Rev. B* **1986**, *33*, 8822−8824.

(27) van Lenthe, E.; Ehlers, A.; Baerends, E. J. *J. Chem. Phys.* **1999**, *110*, 8943−8953.

(28) (a) van Gisbergen, S. J. A.; Groeneveld, J. A.; Rosa, A.; Snijders, J. G.; Baerends, E. J. *J. Phys. Chem. A* **1999**, *103*, 6835−6844. (b) Rosa, A.; Baerends, E. J.; van Gisbergen, S. J. A.; van Lenthe, E.; Groeneveld, J. A.; Snijders, J. G. *J. Am. Chem. Soc.* **1999**, *121*, 10356−10365. (c) van Gisbergen, S. J. A.; Rosa, A.; Ricciardi, G.; Baerends, E. J. *J. Chem. Phys.* **1999**, *111*, 2499−2506.

(29) (a) Klamt, A.; Schüürmann, G. *J. Chem. Soc., Perk. Trans. 2* **1993**, 799−805. (b) Klamt, A. *J. Phys. Chem.* **1995**, *99*, 2224−2235. (c) Klamt, A.; Jonas, V. *J. Chem. Phys.* **1996**, *105*, 9972−9981. (d) Pye, C. C.; Ziegler, T. *Theor. Chem. Acc.* **1999**, *101*, 396−408.

(30) Reid, R. C.; Prausnitz, J. M.; Poling, B. E. *The Properties of Gases and Liquids*, 4th ed.; McGraw-Hill International: New York, 1987.

(31) Bondi, A. *J. Phys. Chem.* **1964**, *68*, 441−451.

(32) Portmann, S.; Lüthi, H. P. *Chimia* **2000**, *54*, 766−770.

(33) http://www.chemcraftprog.com/index.html. (Accessed March 1, 2009).

(34) O'Boyle, N. M.; Tenderholt, A. L.; Langner, K. M. *J. Comput. Chem.* **2008**, *29*, 839−845.

(35) In the Results and Discussion section describing the results of cyclovoltammetric and spectroelectrochemical investigations, the prefixes mer- and trans- are not used when discussing *mer*-$[Os^{III}(CO)(bpy)Cl_3]$ and *trans*(Cl)-$[Os(CO)(PrCN)(bpy)Cl_2]$. The reason is an uncertainty when attributing geometries to the corresponding Os- and bpy-reduced species, such as $[Os^{II}(CO)(bpy^{\bullet-})Cl_3]^{2-}$ (see the discussion to Figure 3).

(36) Pruchnik, F. P.; Galdecka, E.; Galdecki, Z.; Kowalski, A. *Polyhedron* **1999**, *18*, 2091−2097.

(37) Jakonen, M.; Hirva, P.; Haukka, M.; Chardon-Noblat, S.; Lafolet, F.; Chauvin, J.; Deronzier, A. *Dalton Trans.* **2007**, 3314−3324.

(38) (a) Krejčík, M.; Vlček, A. A. *J. Electroanal. Chem.* **1991**, *313*, 243−257. (b) Víchová, J.; Hartl, F.; Vlček, A. *J. Am. Chem. Soc.* **1992**, *114*, 10903−10910.

(39) van Outersterp, J. W. M.; Hartl, F.; Stufkens, D. J. *Organometallics* **1995**, *14*, 3303−3310.

(40) Cheng, S. C.; Blaine, C. A.; Hill, M. G.; Mann, K. R. *Inorg. Chem.* **1996**, *35*, 7704−7708.